



HAL
open science

Passive Chaos Bandwidth Enhancement Under Dual-Optical Feedback with Hybrid III–V/Si DFB Laser

Kevin Schires, Sandra Gomez, Antonin E Gallet, Guang-Hua Duan, Frederic Grillot

► **To cite this version:**

Kevin Schires, Sandra Gomez, Antonin E Gallet, Guang-Hua Duan, Frederic Grillot. Passive Chaos Bandwidth Enhancement Under Dual-Optical Feedback with Hybrid III–V/Si DFB Laser. IEEE Journal of Selected Topics in Quantum Electronics, 2017, 23 (6), pp.1801309. 10.1109/JSTQE.2017.2732830 . hal-02101630

HAL Id: hal-02101630

<https://hal.science/hal-02101630>

Submitted on 17 Apr 2019

HAL is a multi-disciplinary open access archive for the deposit and dissemination of scientific research documents, whether they are published or not. The documents may come from teaching and research institutions in France or abroad, or from public or private research centers.

L'archive ouverte pluridisciplinaire **HAL**, est destinée au dépôt et à la diffusion de documents scientifiques de niveau recherche, publiés ou non, émanant des établissements d'enseignement et de recherche français ou étrangers, des laboratoires publics ou privés.

Passive Chaos Bandwidth Enhancement Under Dual-Optical Feedback with Hybrid III–V/Si DFB Laser

Kevin Schires, Sandra Gomez, Antonin Gallet, Guang-Hua Duan, *Senior Member, IEEE*, and Frédéric Grillot

Abstract—The chaotic dynamics of a DFB laser are studied experimentally under a combination of short and long feedbacks. Chaos bandwidth enhancement is demonstrated using a hybrid III–V/Si DFB laser with a large relaxation oscillation frequency (ROF) of 14 GHz. The impact of short feedback on the ROF is studied and an increase of 2 GHz is observed. Under long feedback, the route to chaos of the device and its dependence on the short feedback dynamics are studied. The short feedback allows tuning the chaotic dynamics obtained under long feedback, and the increase of the ROF translates into an enhancement of the chaos bandwidth to above 16 GHz. This configuration can allow generation of wideband chaos using a single laser source in a photonic integrated circuit.

Index Terms—III–V materials, nonlinear dynamics, optical feedback, silicon photonics, secure communications.

I. INTRODUCTION

SILICON photonics offer tight integration of a variety of active and passive optical and electrical components, and gained so much interest in the last decade that it is now considered one of the most promising technology for optical applications [1], [2]. Building on the mature fabrication techniques first developed for microelectronics allows creating photonic integrated circuits (PICs) with a high density of optical components, in high volumes and at low costs. Academic and industrial efforts led to the development of novel technical solutions for a variety of domains including sensing, measurement instrumentation, optical signal processing and telecommunications

Manuscript received February 7, 2017; revised March 30, 2017 and June 29, 2017; accepted June 30, 2017. This work was supported by the European Union Horizon 2020 Programme under the PICs4All Project (<http://www.pics4all.jeppix.eu>). (Corresponding author: Kevin Schires.)

K. Schires and S. Gomez are with Télécom ParisTech, Université Paris-Saclay, Paris 75634, France (e-mail: schires@enst.fr; sandra.gomez@telecom-paristech.fr).

A. Gallet is with Télécom ParisTech, Université Paris-Saclay, Paris 75634, France, and also with the III–V Lab, Joint Laboratory of Nokia Bell Labs, Thales Research and Technology, and CEA-Leti, Fresnel 91767, France (e-mail: antonin.gallet@3-5lab.fr).

G.-H. Duan are with the III–V Lab, Joint Laboratory of Nokia Bell Labs, Thales Research and Technology, and CEA-Leti, Fresnel 91767, France (e-mail: guanghua.duan@3-5lab.fr).

F. Grillot is with Télécom ParisTech, Université Paris-Saclay, Paris 75634, France, and also with the Center for High Technology Materials, University of New Mexico, Albuquerque, NM 87106-4343 USA (e-mail: grillot@telecom-paristech.fr).

Color versions of one or more of the figures in this paper are available online at <http://ieeexplore.ieee.org>.

Digital Object Identifier 10.1109/JSTQE.2017.2732830

[3], [4]. Recent advances in data centers and informatics [5] reveal how photonic integration will become increasingly used for data transmission, either inside a chip or for short-access and long-haul telecommunications networks [6], [7].

Each discrete component used in electro-optical devices had to be redesigned for integration on Si, and a number of research works allowed developing novel integrated modulators, photodetectors, isolators, polarization controllers, amplifiers, as well as novel laser sources [8]. As laser cavities had to be adapted for integration into PICs, novel fabrication techniques were derived for the growth of the active material, and novel designs of the resonant cavity were proposed [9]–[12]. The active III–V material is generally not grown directly on a Si substrate but rather wafer bonded onto a Si waveguide: lattice mismatches between III–V compounds and Si as well as different thermal expansion lead to dislocation in Quantum Well (QW) materials and to poor device reliability. Novel Quantum Dot (QD) laser sources grown directly on Si have recently been reported [13], [14]: unlike QW materials, the localization of carriers in QDs make these less sensitive to defects. Complex laser cavities for single and multimode laser sources have been proposed [15], but such designs were shown to suffer from stability issues due to internal feedback sources [16] and a simpler DFB structure is studied in this work.

Multisection lasers have been demonstrated on PICs, and devices with an integrated external feedback cavity for use as chaotic emitters are of interest for both academic and industrial research [17]–[19]. PICs creating an external cavity with a phase section are important for research purposes as they allow study of the behavior of lasers under optical feedback with short cavities of controllable length, thus giving new insights into laser dynamics [20], [21]. Under optical feedback of increasing strength, the laser’s relaxation oscillations become excited and lead to chaotic oscillation of the laser output [22]. PICs containing lasers with and external optical feedback cavity are thus very important for practical applications, as they allow the use of chaotic emitters in communication networks without imposing volume constraints for integration into existing emitter and receiver modules.

Two major applications of chaotic emitters in communication networks are random number generation and most importantly secure communications [23]. Chaotic communications rely on hiding data within a broad chaotic spectrum at the emitter level, and the data is recovered in the receiver. The bandwidth of the

76 amplified feedback should thus be maximized to increase trans-
 77 mission rates while keeping the data secure, and several schemes
 78 were proposed to obtain large chaos bandwidth, defined as the
 79 frequency under which 80% of the RF power is found [24]. Pas-
 80 sive enhancement of the chaos bandwidth was proposed using
 81 phase-conjugate feedback and a high-reflectivity mirror [25].
 82 Active solutions using optical injection from two laser sources
 83 in addition to optical feedback demonstrated chaos bandwidths
 84 as high as 32 GHz [26].

85 Another way of generating broad chaos is to increase the
 86 relaxation oscillation frequency (ROF) of the laser source.
 87 Under optical feedback, the generated chaotic spectra scale
 88 with the relaxation frequency of the laser, as chaotic dynamics
 89 build up from enhanced relaxation oscillations. In addition, the
 90 ROF can be tuned using optical feedback, depending on the
 91 feedback phase and strength [22], [27], [28], and that dynamics
 92 can be generated by tailoring the feedback and controlling its
 93 phase [29]. It was demonstrated that PICs with an integrated
 94 amplified external cavity with a phase section allowed forcing
 95 self-pulsations in the laser at a frequency tuneable to above
 96 40 GHz [30], [31].

97 In this article, we study the enhancement of the bandwidth of
 98 chaotic dynamics using a combination of two passive cavities of
 99 different scales. Chaos bandwidth enhancement is demonstrated
 100 using a hybrid III-V/Si QW DFB laser in order to prove appli-
 101 cations to PICs. As the optical cavities are created in a fibered
 102 setup and not within the chip, only low feedback strengths are
 103 achieved. This study shows for the first time the evolution of
 104 the dynamics of a hybrid III-V/Si DFB laser with the strength
 105 of a long feedback or the phase of a short feedback, and combi-
 106 nations of the two. In Section I, the device is presented and
 107 characterized, and the impact of internal reflections on laser
 108 operation is discussed. The free-running laser exhibits high re-
 109 laxation oscillations of 14 GHz which make it ideal for this study
 110 as large ROF simplifies the access to wide chaos bandwidths.
 111 The route to chaos of the hybrid laser under long feedback is
 112 studied in Section III, and compared with that of a commercial
 113 III-V DFB laser, showing similar behaviors between the two
 114 types of laser despite significant differences in their structures.
 115 In Section IV, the laser is subject to a short feedback cavity
 116 which allows increasing its ROF by 2 GHz. In Section V, the
 117 laser is subject to both feedback cavities, and the chaos band-
 118 width is found to be enhanced in the same fashion as the ROF.
 119 The chaos bandwidth is increased by up to 13% and reaches a
 120 maximum of 16.4 GHz, showing that this combination of two
 121 feedbacks allows controlling the bandwidth and characteristics
 122 of the generated chaos despite the very low feedback strength
 123 allowed by the setup. Such passive chaos bandwidth enhance-
 124 ment can be applied to standard III-V DFB lasers, and the setup
 125 is transposable to a PIC constituted of the laser and two cavities
 126 with optional phase sections, allowing wide chaos generation
 127 with low power consumption.

128 II. EXPERIMENTAL APPARATUS

129 A. Device Studied

130 Fig. 1 presents a schema of the DFB structure studied. The
 131 1 mm-long hybrid III-V Silicon-on-Insulator (SOI) device is

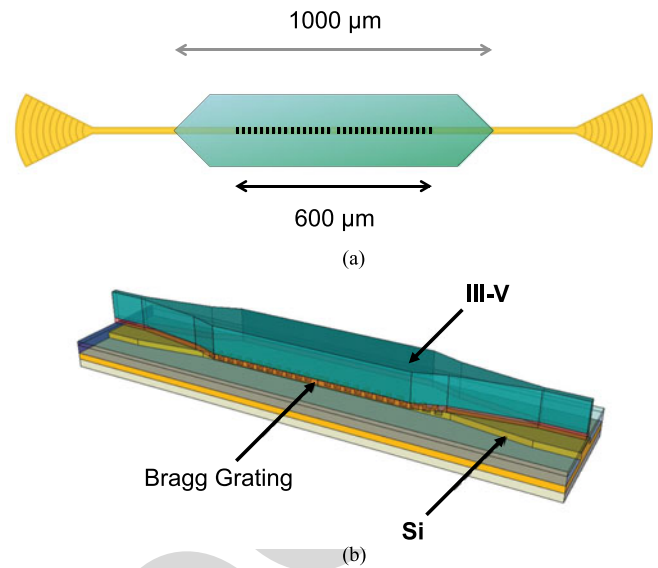


Fig. 1. (a) Schematic and (b) structure of the device studied, showing the Si waveguide (yellow) and the III-V material (green). The vertical couplers are represented in (a) at both extremities of the Si waveguide.

132 fabricated using a III-V QW active medium bonded on top of
 133 the processed silicon waveguide, and constituted of a DFB laser
 134 with tapers on each side [15]. To ensure single-mode operation,
 135 a 50 nm-deep and 600 μm-long Bragg grating with a quarter-
 136 wavelength phase shift in the center is etched on the silicon
 137 waveguide. The strength of the grating is chosen such that the
 138 product κL_{bragg} is of a few units, and the period of the grating
 139 is of 240 nm. The light is coupled from the Si waveguide to the
 140 III-V material with adiabatic tapers, and outcoupled using Verti-
 141 cal Bragg Gratings (VBG) on both side of the device. The VBG
 142 couples the light out of the laser with an angle of 80° from the
 143 waveguide, and light was thus coupled vertically using a fiber
 144 positioned above the laser, with a 10° angle from the normal
 145 to the lasers surface. The VBG were only necessary for testing
 146 purposes, in order to characterize several unprocessed devices
 147 on the same bar, and in a PIC they would not be positioned after
 148 the laser. They however affected our study in two ways: first via
 149 their transmission losses of approximately 7 dB, which will be
 150 discussed later, and secondly by their parasitic reflectivity (be-
 151 low -23 dB) which affected laser operation when biased high
 152 above threshold.

153 B. Characterisation

154 Fig. 2(a) presents the evolution of the power coupled into an
 155 anti-reflection (AR)-coated lens-ended fiber with the bias cur-
 156 rent. All measurements presented in this paper were performed
 157 at 20 °C. Around the threshold of about 45 mA, the laser ex-
 158 hibits slight competition between two modes which translates
 159 into a kink in the curve. Between 50 and 150 mA, very stable
 160 single-mode operation is observed with a side-mode suppression
 161 ratio above 50 dB. Above 4 times threshold, the laser exhibited
 162 power drops which were also observed on the other lasers of
 163 the same bar, but differed from device to device. Such behavior
 164 hints that parasitic reflections are present within the devices:
 165 the vertical couplers and tapers create reflections which only

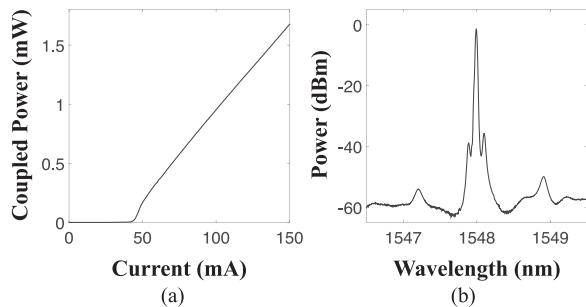


Fig. 2. (a) Evolution of the power coupled using an AR-coated lensed fiber with the pump current. (b) Optical spectrum at a bias current of 140 mA.

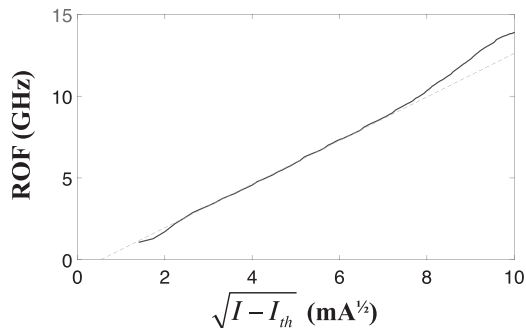


Fig. 3. Evolution of the ROF with the square root of the current overdrive above threshold.

166 seem to affect the laser far above threshold through variations
 167 of the optical power or changes in the ROF, as will be discussed
 168 next. As the amount of parasitic reflections varies from device
 169 to device, different sorts of power variation would indeed be
 170 expected between the different lasers. Fig. 2(b) presents the
 171 spectrum of the laser at 140 mA, showing the well-suppressed
 172 side-modes as well as sidebands characteristic of relaxation oscil-
 173 lations. These spectra were measured using a Yenista OSA20
 174 optical spectrum analyzer with a 20 pm resolution, and these
 175 sidebands could be measured thanks to the rather high value of
 176 the ROF.

177 Fig. 3 presents the evolution of the ROF as a function of the
 178 square root of the current overdrive above threshold. It can
 179 be noted that very high frequencies are observed as the ROF
 180 reaches 14 GHz at 150 mA. Usually, due to gain compression,
 181 the power evolves in a sublinear fashion with increasing bias
 182 current, and the squared ROF follows the same trend. Here, it
 183 can be seen that the ROF rather evolves in the opposite way as
 184 it gradually increases above the linear fitting shown as a dashed
 185 line.

186 We believe that these high values of ROF stem from the use
 187 of Aluminium in the III-V compound forming the QW [32], but
 188 also from the aforementioned internal feedback. Under optical
 189 feedback, the ROF can oscillate around its free-running value
 190 depending on the feedback strength and delay [22]. Here, the
 191 internal feedback conditions thus allow a small enhancement of
 192 the ROF for some bias currents, showing an effect of parasitic
 193 feedback very different from the detrimental impact it can have
 194 further above threshold.

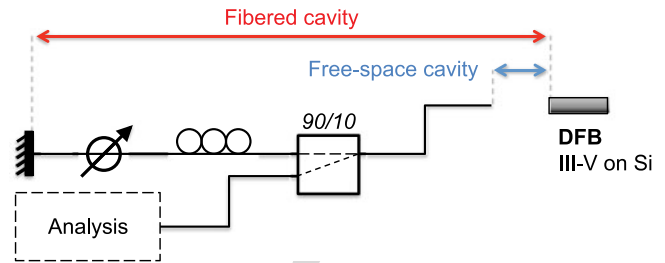


Fig. 4. Experimental setup allowing combination of short and long feedback.

C. Experimental Setup

195

196 Fig. 4 presents the experimental setup used for the following
 197 measurements [16]. The DFB is kept at a bias current of 146 mA
 198 and at 20 °C. The light of the DFB laser is coupled using either an
 199 AR-coated lensed fiber or a cleaved uncoated one. The cleaved
 200 fiber allows creating a short free-space feedback cavity [33] of
 201 the order of 100 μm , re-injecting about 3% of the light back
 202 into the device with a time delay below 1 ps. On the other hand,
 203 the lens-ended fiber minimizes such reflections and only
 204 allows light from the setup to be re-injected into the device. In
 205 the fiberized setup, a 90/10 splitter is used to create a feedback
 206 path consisting of a polarization controller and a Yenista Back-
 207 Reflector (BKR) module, equivalent to a mirror with variable
 208 losses. This long fibered cavity measures approximately 7 m
 209 and allows re-injecting at most 8% of the light into the device.
 210 Note that due to the transmission losses of the vertical couplers,
 211 a difference must be made between the light re-injected into the
 212 component and the light that reaches the laser cavity. The
 213 maximum feedback strengths considering the light that reaches
 214 the laser cavity are thus of 0.1% and 0.3% for the short and long
 215 cavities, respectively.

216 Using either fiber and controlling the attenuation of the long
 217 feedback path allows studying the laser into the following four
 218 situations: free-running with only parasitic reflections from
 219 the setup, under short (free-space) feedback only, under long
 220 (fibered) feedback only, and under a combination of both feed-
 221 backs. For the short feedback, while the feedback strength is
 222 fixed by the refractive index of the fiber, the phase can be tuned
 223 using a piezoelectric actuator allowing gradually moving the
 224 fiber towards or away from the device. Concerning the long
 225 feedback, while the feedback phase can be changed the same
 226 way it does not impact laser behavior given the large external
 227 cavity length. Feedback strength can however be tuned by
 228 changing the attenuation of the BKR.

III. LONG FEEDBACK

229

230 To assess the potential of such hybrid lasers as chaotic emit-
 231 ters, we first study the route to chaos that the devices follow
 232 under long feedback. The cavity used here is too long to repre-
 233 sent the external cavity that would be integrated in a PIC, but it
 234 allows pushing the laser into chaotic operation where the phase
 235 of the long feedback has little impact on the dynamics. This
 236 will later allow us to dissociate the effect of the short and long
 237 feedbacks when combined together, as we can consider that the
 238 feedback phase will only affect the dynamics induced by the

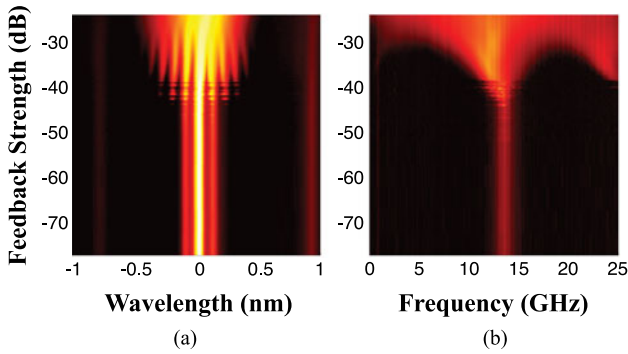


Fig. 5. Evolution of the (a) optical and (b) RF spectra with long feedback strength, using a lens-ended fiber.

short feedback. Fig. 5 presents the evolution of the optical and RF spectra with the long feedback strength, using the lensed fiber. The measurements performed with the lensed fiber have very little dependence on the position of the fiber and thus the feedback phase, as it will be shown later in the case of the free-running laser. Routes to chaos under long feedback were thus found to be identical for different positions of the fiber.

The route observed is typical of a DFB laser under long optical feedback despite major differences in the device structures: first of all, the hybrid DFB is constituted of two evanescently coupled waveguides, one passive and one active, unlike the standard III-V DFB. In addition, in the hybrid device the tapered regions on each side of the DFB structure may slightly amplify the light fed back into the laser, or even act as source of internal reflections [16]. The proposed chaos bandwidth enhancement method could also be applied to a standard III-V DFB, for which higher feedback strengths could be achieved. Demonstrating the changes in ROF and bandwidth in the case of hybrid lasers is however interesting, as it shows that the complexity of the lasers used in PICs does not necessarily affect their behavior under optical feedback.

For very low feedback strengths, the ROF can be seen at 14 GHz in the RF spectrum. Around -43 dB of feedback strength, temporally unstable periodic oscillations start to appear, and stabilize above -40 dB. These correspond to an excitation of relaxation oscillations that turn into chaotic dynamics above -30 dB of feedback strength. Under maximum feedback strength, the bandwidth of the chaotic spectra is of 14.5 GHz.

Fig. 6 allows comparing the route to chaos of this hybrid DFB laser with that of a commercial Nokia III-V DFB laser. The laser is operated a three times its threshold where it has a ROF of 8 GHz. The routes appear to be very similar. Along the feedback strength axis, the routes appear to be shifted by 6 dB as the III-V DFB reaches chaotic operation for only -36 dB of feedback strength. Note that in the case of the III-V laser, higher feedback strengths were achievable with the same setup as there were no extra losses between the fiber and the laser cavity. It can thus be seen that with the hybrid DFB we are only able to merely enter the chaotic regime, and that much broader spectra could be observed for stronger feedback. Along the wavelength axis, broader spectra are observed for the hybrid DFB in the region of periodic oscillations, as the base frequency of these oscillations

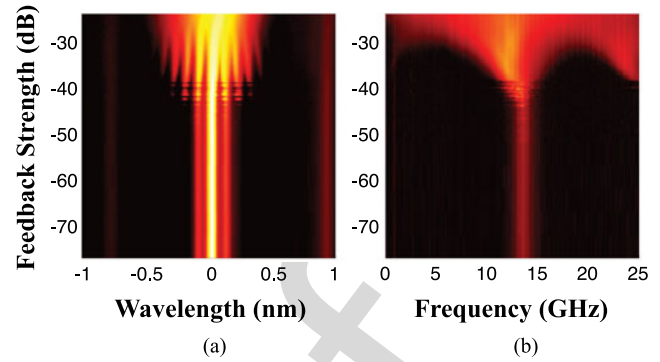


Fig. 6. Evolution of the optical spectra of a (a) III-V and (b) III-V/Si DFB laser with long feedback strength, using a lens-ended fiber.

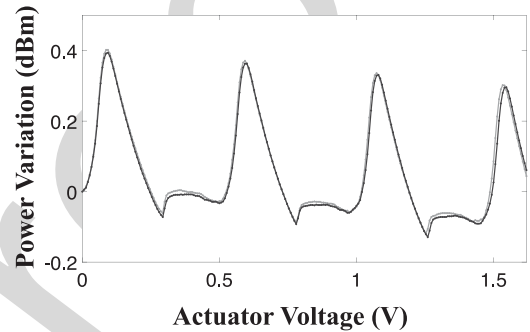


Fig. 7. Variation of the power coupled with the cleaved fiber as a function of the voltage applied to the piezoelectric actuator. Two measurements for different fiber positions are presented in black and grey.

is the ROF, and we expect that the spectra observed for the III-V DFB could be obtained for the hybrid one, broadened by a factor close to the ratio between the two ROFs.

IV. SHORT FEEDBACK

Using the cleaved fiber and setting the long feedback strength to its minimum of -79 dB allows studying the DFB under short feedback only. Fig. 7 presents the variation of the coupled power as a function of the voltage applied to the piezoelectric actuator. As the coupling is only optimized for a voltage of 0 V, the power fades as the fiber is moved away from the device and the figure appears skewed. A clear periodicity can however be observed in the evolution of the power, as we are varying the phase of the short feedback. For convenience, we choose as beginning of each period the main peaks and consider that between each peak, the phase is varied from 0 to 2π . Note that this does not represent the absolute phase of the feedback, but only a representation of the phase shift within a period.

Such variation of the output power under optical feedback corresponds to the effect of a medium feedback strength and usually exhibits bistability when the mirror is moved one way or the other [22]. Fig. 8 presents a comparison between the evolution of the power and spectrum when the fiber is moved in both directions, as well as reference measurements performed with the lensed fiber. The reference measurements shows the weak impact of all parasitic reflections from the setup, and shows that the cavity created by the cleaved fiber is mainly responsible

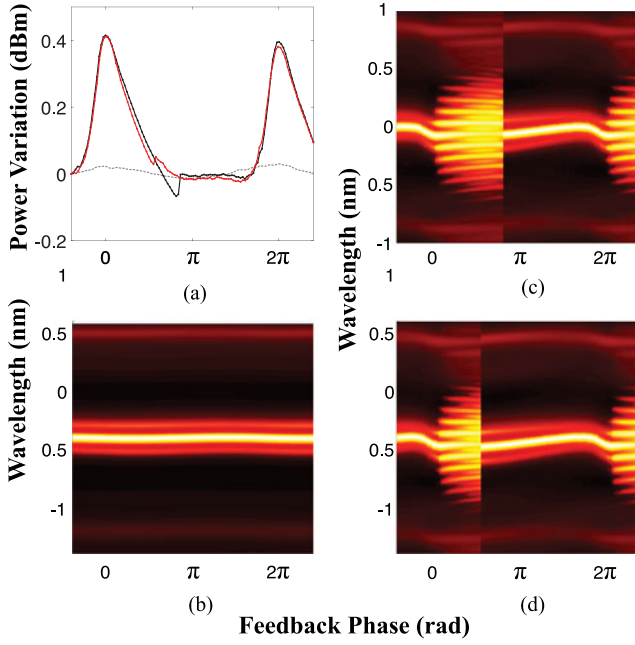


Fig. 8. (a) Variation of the power coupled with the cleaved fiber within one period when the fiber is moved away (black) or towards (red) the laser. The grey dashed line represents the power coupled when using the lensed fiber. (b) Evolution of the optical spectrum when using the lensed fiber. (c) and (d) Show the evolution of the optical spectrum when moving the fiber away or towards the laser, respectively.

307 for the power variation presented above. In Fig. 8(a) the gray
 308 dashed line shows that the power is oscillating sinusoidally
 309 with a low amplitude, which corresponds to the impact of weak
 310 feedback. Fig. 8(b) shows that the wavelength varies in a similar
 311 fashion. This confirms that any other variation of the power or
 312 wavelength is only due to the feedback created by the cleaved
 313 fiber. Fig. 8(a) also reveals a slight bistability in the evolution
 314 of the power, as the kinks observed after the peak occur for
 315 a phase shift of 0.3π for one direction and 0.4π for the other.
 316 While the bistability in the output power is negligible, it makes
 317 a significant difference in the optical spectrum. Note that all
 318 spectrum maps presented in this work are plotted in dBm, with
 319 a logarithmic color scale.

320 Fig. 8(c) reveals that during each periods, the laser exhibits
 321 periodic dynamics between phases of 0 and 0.4π , with period
 322 doubling above 0.2π . When the kink occurs in the optical power,
 323 the laser suddenly stabilises, and it can be seen from the side-
 324 bands that the ROF changes with the phase. Fig. 8(d) shows that
 325 the same behaviour is observed when the fiber is moved in the
 326 opposite direction, thus leading to a wider region of stability.
 327 This wider region is of importance for this study as it appears
 328 that the largest ROFs are achieved within the bistability window
 329 when the laser is stable, as this is where the mode's sidebands
 330 appear to be the farthest apart.

331 Fig. 9 shows the evolution of the optical and RF spectra of the
 332 DFB as the fiber is moved towards the laser, at a shorter distance.
 333 In order to clearly see the peak of the relaxation oscillations in
 334 the RF spectra, an EDFA set to a fixed output power of 10 dBm
 335 was used to amplify the light before detection. A photodetector
 336 with a bandwidth of 30 GHz and a Rohde & Schwartz FSP

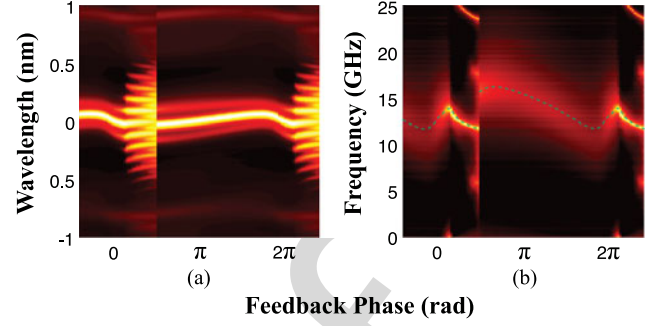


Fig. 9. Evolution of the (a) optical and (b) RF spectra within one period. The green dashed line shows the evolution of the ROF.

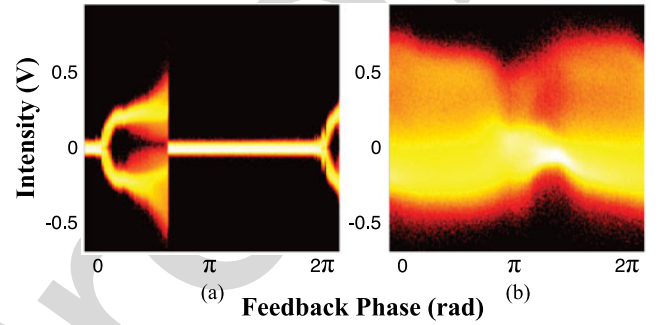


Fig. 10. Bifurcation diagrams as a function of the short feedback phase under (a) minimum and (b) maximum long feedback strength.

40 GHz electrical spectrum analyzer were used to perform the
 337 spectrum measurements. A slightly larger stability region is
 338 obtained, and the RF spectra show that within one period, the
 339 ROF varies between a minimum of 11 GHz and a maximum of
 340 16 GHz, thus allowing reaching frequencies 2 GHz higher than
 341 the free-running ROF.
 342

V. COMBINATION OF FEEDBACKS 343

Under long feedback only, the hybrid DFB exhibits a classic
 344 route to chaos where chaotic dynamics are obtained from the
 345 excitation of relaxation oscillations. Under short feedback only,
 346 it is possible to tune the value of the ROF while keeping the laser
 347 into stable operation. Combining both feedbacks will allow us to
 348 study whether the enhancement of the ROF under short feedback
 349 can be used to generate broader chaos by first tailoring the ROF
 350 and then exciting relaxation oscillations into chaotic ones. In
 351 this section, the laser is thus subjected to a combination of short
 352 and long feedbacks by using the cleaved fiber and varying the
 353 long feedback strength.
 354

Fig. 10 presents the bifurcation diagrams of the dynamics as
 355 a function of the phase of the short feedback, under minimum
 356 and maximum long feedback strengths. Under minimum long
 357 feedback strength, the diagram clearly shows the apparition of
 358 the periodic oscillations and the sudden transition from oscil-
 359 lating to stable operation. Under maximum feedback, it can be
 360 seen that the chaotic signal changes significantly with the short
 361 feedback phase.
 362

Fig. 11 presents the evolution of optical and RF spectra with
 363 the position of the cleaved fiber for four levels of long feedback
 364

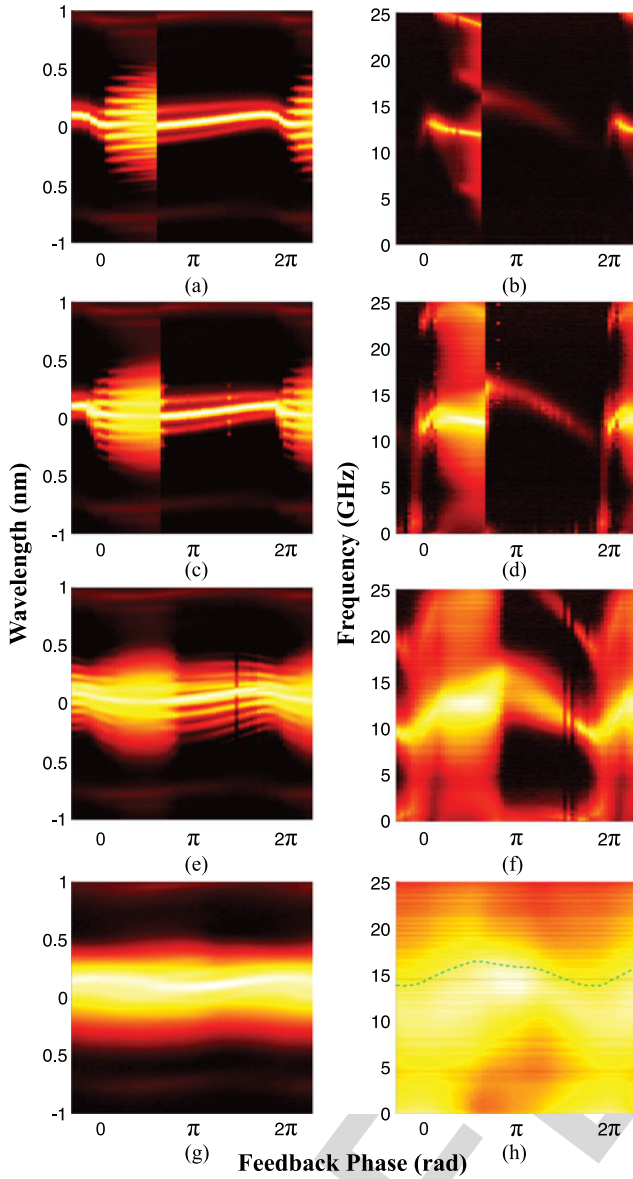


Fig. 11. Evolution of optical (left) and RF (right) spectra with the position of the cleaved fiber for long feedback strengths of (a), (b) -79 dB, (c), (d) -42 dB, (e), (f) -36 dB and (g), (h) -26 dB. In (h) the black line shows the chaos bandwidth under long feedback only, and the green dashed line shows the evolution of chaos bandwidth with the phase of the short feedback.

365 strength: the minimum of -79 dB, -42 dB, -36 dB and the
 366 maximum of -26 dB. No optical amplification was used for
 367 the RF spectrum measurements. The route towards chaos under
 368 long feedback clearly changes with the short feedback phase, as
 369 periodic dynamics appear for different long feedback strengths at
 370 the different positions of the cleaved fiber. Regions where
 371 periodic oscillations occur under short feedback alone appear
 372 to enter chaotic operation first. The sharp transition between
 373 oscillating and stable operation gradually disappears as the long
 374 feedback strength is increased. In a similar way as in Figs. 5
 375 and 6, some points exhibit temporally unstable dynamics for
 376 feedback phases between 1.3π and 1.5π and feedback strengths
 377 of -42 and -36 , which can be seen as a disappearance of the

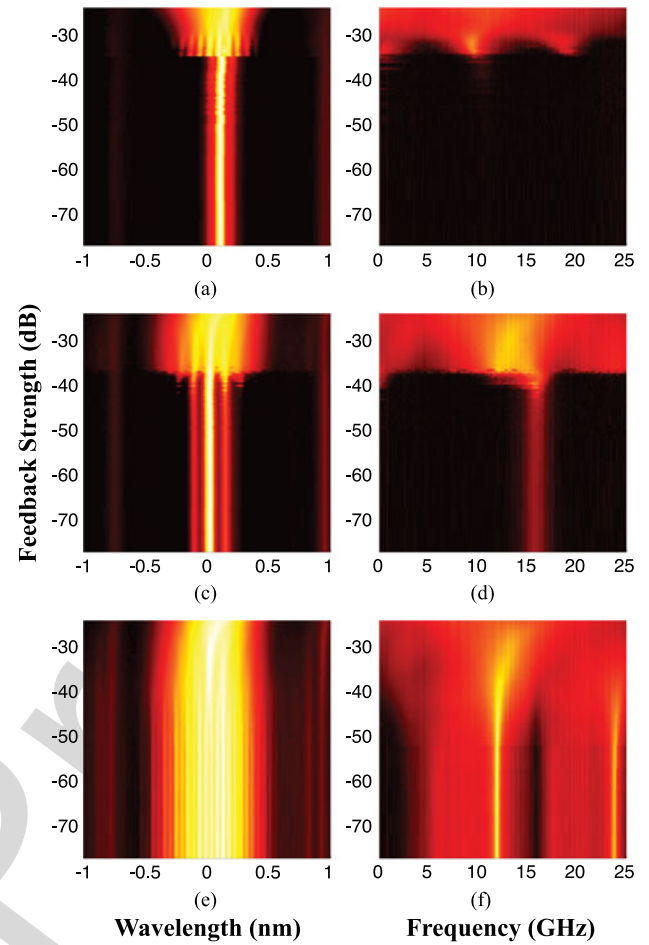


Fig. 12. Evolution of the optical (left) and RF (right) spectra with the long feedback strength for three positions of the cleaved fiber. (a) and (b) correspond to a feedback phase of 1.9π (minimum ROF, stable). (c) and (d) correspond to a feedback phase of 0.3π (maximum ROF, stable). (e) and (f) correspond to a feedback phase of 0.25π (strongest oscillations).

dynamics for some isolated feedback phases. It is interesting
 to observe that, as the long feedback strength is increased, the
 wavelength of the spectrum peak oscillates in a more and more
 sinusoidal fashion, such that no bistability was observed under
 maximum long feedback strength.

The long feedback strength necessary to reach chaotic operation
 seems to depend on the short feedback phase, and it can be
 seen in Fig. 11(g) and (h) that the width of the chaotic spectrum
 varies with the feedback phase too. In Fig. 11(h), the super-
 imposed green dashed line shows the evolution of the chaos
 bandwidth with the short feedback phase. The black dotted line
 shows as a reference the bandwidth of the chaos measured under
 maximum long feedback only, corresponding to the spectrum
 under maximum long feedback strength in Fig. 5(b). With the
 addition of short feedback, the chaos bandwidth oscillates be-
 tween 13.7 and 16.4 GHz by following very closely the evolu-
 tion of the ROF in Fig. 9(b). Minimum and maximum chaos
 bandwidth are indeed respectively found close to the feedback
 phases where minimum and maximum ROF are observed in the
 absence of long feedback.

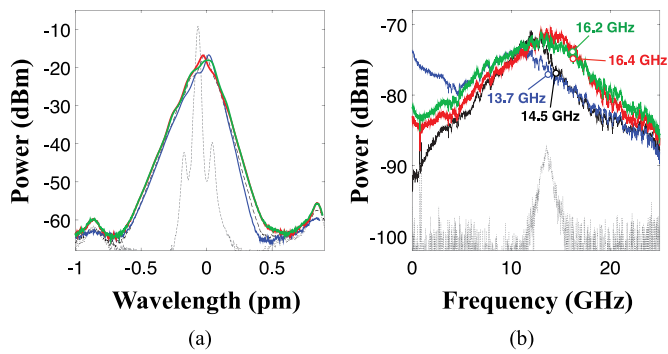


Fig. 13. Optical (left) and RF (right) spectra under maximum long feedback and their bandwidth, the dashed lines showing the free-running spectra as reference. The black curve corresponds to maximum long feedback alone. The blue (resp. red) curve corresponds to both feedbacks with minimum (maximum) ROF. The green curve corresponds to both feedback with strongest periodic oscillations.

398 Three specific routes to chaos are thus of interest: those where
 399 short feedback does not destabilize the laser but induces either
 400 a reduction of the ROF to its minimum value of 11 GHz (phase
 401 of 1.9π) or an increase to its maximum value of 16 GHz (phase
 402 of 0.3π), and one where short feedback induces the strongest
 403 periodic oscillations (phase of 0.25π). Fig. 12 presents these
 404 three routes. In the first two routes, the laser remains stable until
 405 slightly higher feedback strengths than compared to Fig. 5(a).
 406 The window where periodic oscillations are observed is however
 407 very narrow, as chaos appears around the same feedback strength
 408 of about -30 dB. In the last route, chaotic dynamics seem to
 409 appear for a lower long feedback strength of -38 dB, but under
 410 maximum long feedback the end of the route appears similar to
 411 that in Fig. 12(d). This is however not surprising given that the
 412 last two routes are measured for short feedback phases that are
 413 rather close, and that no discontinuity can be seen in Fig. 11(g)
 414 and (h) between these phases.

415 The optical and RF spectra obtained under maximum long
 416 feedback for these three operating conditions are shown in
 417 Fig. 13, along with the free-running spectra and the chaotic
 418 ones obtained under maximum long feedback alone. Fig. 13(b)
 419 shows that the chaotic spectrum obtained for a feedback phase
 420 of 1.9π leads to the minimum bandwidth of 13.7 GHz observed
 421 in Fig. 11(h). Both the other routes lead to a bandwidth of
 422 16.2 GHz, despite slight differences in the chaotic spectra.

423 VI. CONCLUSION

424 A combination of long and short feedback are used to respec-
 425 tively generate chaotic dynamics in a DFB laser and tune the
 426 chaos bandwidth. The dynamics of a hybrid III-V/Si DFB laser
 427 were studied under such combination of feedbacks to show the
 428 possibility to achieve passive chaos bandwidth enhancement in
 429 PICs. The routes of the dynamics are extensively characterized
 430 by varying the phase of the short feedback and strength of the
 431 long one. Owing to the large ROF of the free-running laser,
 432 chaotic dynamics with a bandwidth of 14.5 GHz can be gener-
 433 ated using a long external feedback cavity. The route to chaos

appears to be very similar to that of a standard commercial III-V
 DFBs, but due to the transmission losses of the device's verti-
 cal couplers, maximum feedback strengths of only 0.3% were
 achievable. The impact of a short external cavity on the laser
 dynamics revealed a variation of the ROF of 5 GHz, with a
 maximum value of 16 GHz. When combining short and long
 feedbacks, this 2 GHz increase of the ROF translates into a simi-
 lar increase of the chaos bandwidth, which reaches 16.4 GHz.

The tuneability of the chaotic dynamics and of their band-
 width is of interest for applications requiring random number
 generation, or broad chaos generation. With feedback cavities
 integrated into a Si waveguide along with a phase section, higher
 feedback strengths would be achievable for both short and long
 feedbacks. Chaotic spectra much wider than those reported in
 this work could thus be obtained using a single component and
 passive optical cavities with optional phase sections. This would
 be of prime importance for the development of low-consumption
 integrated chaotic transmitters and receivers for secure commu-
 nications.

As the wide bandwidth relies primarily on the large ROF
 of the laser, the design of the device is extremely important,
 and for these applications QW sources may be more appealing
 than QD sources as QW lasers generally exhibit much higher
 ROFs than QD ones. In the case of application in a Si PIC, the
 design of the Si waveguides would be very important too, as all
 the possible sources of reflections within the PIC will affect the
 dynamics of the laser. In this work, at least two feedback cavities
 allow pushing the ROF towards the values reported here: the
 cavity created by the cleaved fiber, but also the internal parasitic
 sources of feedback which seem to increase the ROF of the
 free-running laser already. If sources of feedback are inevitable
 in a PIC, they can thus be designed to potentially enhance the
 laser's operation instead of hindering it.

Future work will focus on the simulation of single mode III-V
 and III-V/Si lasers subject to two external cavities in order to
 attempt to replicate these experimental results. Conditions to
 maximize the increase of the ROF under short feedback will
 thus be studied in the presence of several short cavities, in order
 to reach larger bandwidth enhancements. It will also be possible
 to determine which absolute feedback phase leads to the wider
 chaos bandwidth, to see if it is phase-conjugate feedback that
 leads to the largest enhancement. Finally, the theoretical results
 should allow identifying the minimum length of the long cavity
 required to achieve sufficient chaos bandwidth, which will
 help the design and realization of an integrated wideband chaos
 generator.

REFERENCES

- [1] D. Thomson *et al.*, "Roadmap on silicon photonics," *J. Opt.*, vol. 18, no. 7, 481
2016, Art. no. 073003. 482
- [2] L. Vivien and L. Pavesi, *Handbook of Silicon Photonics*. Boca Raton, FL, 483
USA: CRC Press, Apr. 2013. 484
- [3] G. Roelkens *et al.*, "Silicon-based heterogeneous photonic integrated 485
circuits for the mid-infrared," *Opt. Mater. Express*, vol. 3, no. 9, 486
pp. 1523–1536, Sep. 2013. 487
- [4] A. Rickman, "The commercialization of silicon photonics," *Nature Pho-* 488
ton., vol. 8, no. 8, pp. 579–582, Aug. 2014. 489

- [5] C. Sun *et al.*, "Single-chip microprocessor that communicates directly using light," *Nature*, vol. 528, no. 7583, pp. 534–538, Dec. 2015.
- [6] M. Asghari and A. V. Krishnamoorthy, "Silicon photonics: Energy-efficient communication," *Nature Photon.*, vol. 5, no. 5, pp. 268–270, May 2011.
- [7] Y. A. Vlasov, "Silicon CMOS-integrated nano-photonics for computer and data communications beyond 100 g," *IEEE Commun. Mag.*, vol. 50, no. 2, pp. s67–s72, Feb. 2012.
- [8] M. J. R. Heck, "Grating coupler enabled optical isolators and circulators for photonic integrated circuits," *IEEE J. Sel. Topics. Quantum Electron.*, vol. 21, no. 4, pp. 361–369, Jul. 2015.
- [9] A. W. Fang *et al.*, "Electrically pumped hybrid AlGaInAs-silicon evanescent laser," *Opt. Express*, vol. 14, no. 20, pp. 9203–9210, Oct. 2006.
- [10] A. W. Fang *et al.*, "Hybrid silicon evanescent devices," *Mater. Today*, vol. 10, no. 78, pp. 28–35, Jul. 2007.
- [11] G. Roelkens *et al.*, "III-V/Si photonics by die-to-wafer bonding," *Mater. Today*, vol. 10, no. 78, pp. 36–43, Jul. 2007.
- [12] H. Park *et al.*, "Device and integration technology for silicon photonic transmitters," *IEEE J. Sel. Topics. Quantum Electron.*, vol. 17, no. 3, pp. 671–688, May 2011.
- [13] A. Y. Liu *et al.*, "High performance continuous wave 1.3 μ m quantum dot lasers on silicon," *Appl. Physics Lett.*, vol. 104, no. 4, Jan. 2014, Art. no. 041104.
- [14] S. Chen *et al.*, "Electrically pumped continuous-wave III-V quantum dot lasers on silicon," *Nature Photon.*, vol. 10, no. 5, pp. 307–311, May 2016.
- [15] G. H. Duan *et al.*, "Hybrid III-V on silicon lasers for photonic integrated circuits on silicon," *IEEE J. Sel. Topics. Quantum Electron.*, vol. 20, no. 4, pp. 158–170, Jul. 2014.
- [16] K. Schires *et al.*, "Dynamics of hybrid III-V silicon semiconductor lasers for integrated photonics," *IEEE J. Sel. Topics Quantum Electron.*, vol. 22, no. 6, pp. 43–49, Nov. 2016.
- [17] A. Argyris, M. Hamacher, K. E. Chlouverakis, A. Bogris, and D. Syvridis, "Photonic integrated device for chaos applications in communications," *Physical Rev. Lett.*, vol. 100, no. 19, May 2008, Art. no. 194101.
- [18] A. Argyris, S. Deligiannidis, E. Pikasis, A. Bogris, and D. Syvridis, "Implementation of 140 Gb/s true random bit generator based on a chaotic photonic integrated circuit," *Opt. Express*, vol. 18, no. 18, pp. 18 763–18 768, Aug. 2010.
- [19] R. Takahashi *et al.*, "Fast physical random bit generation with photonic integrated circuits with different external cavity lengths for chaos generation," *Opt. Express*, vol. 22, no. 10, pp. 11 727–11 740, May 2014.
- [20] A. K. Dal Bosco *et al.*, "Cycles of self-pulsations in a photonic integrated circuit," *Physical Rev. E*, vol. 92, no. 6, Dec. 2015, Art. no. 062905.
- [21] A. K. Dal Bosco *et al.*, "Photonic integrated circuits unveil crisis-induced intermittency," *Opt. Express*, vol. 24, no. 19, pp. 22 198–22 209, Sep. 2016.
- [22] J. Ohtsubo, *Semiconductor Lasers: Stability, Instability and Chaos*. New York, NY, USA: Springer-Verlag, 2013.
- [23] A. Argyris *et al.*, "Chaos-based communications at high bit rates using commercial fibre-optic links," *Nature*, vol. 438, no. 7066, pp. 343–346, Nov. 2005.
- [24] H. Someya, I. Oowada, H. Okumura, T. Kida, and A. Uchida, "Synchronization of bandwidth-enhanced chaos in semiconductor lasers with optical feedback and injection," *Opt. Express*, vol. 17, no. 22, pp. 19 536–19 543, Oct. 2009.
- [25] A. Mercier, D. Wolfersberger, and M. Sciamanna, "Improving the chaos bandwidth of a semiconductor laser with phase-conjugate feedback," *Proc. SPIE*, vol. 9892, 2016, Art. no. 98 920G.
- [26] M. Zhang *et al.*, "Generation of broadband chaotic laser using dual-wavelength optically injected Fabry-Perot laser diode with optical feedback," *IEEE Photon. Technol. Lett.*, vol. 23, no. 24, pp. 1872–1874, Dec. 2011.
- [27] D. Lenstra, "Relaxation oscillation dynamics in semiconductor diode lasers with optical feedback," *IEEE Photon. Technol. Lett.*, vol. 25, no. 6, pp. 591–593, Mar. 2013.
- [28] D. D'Agostino, H. P. M. M. Ambrosius, M. K. Smit, and D. Lenstra, "Integrated laser with optical feedback shows suppressed relaxation-oscillation dynamics," *IEEE Photon. Technol. Lett.*, vol. 27, no. 21, pp. 2292–2295, Nov. 2015.
- [29] J. Zhao *et al.*, "Stability of a monolithic integrated filtered-feedback laser," *Opt. Express*, vol. 20, no. 26, pp. B270–B278, Dec. 2012. [Online]. Available: <https://www.osapublishing.org/abstract.cfm?uri=oe-20-26-B270>
- [30] O. Brox *et al.*, "High-frequency pulsations in DFB lasers with amplified feedback," *IEEE J. Quantum Electron.*, vol. 39, no. 11, pp. 1381–1387, Nov. 2003.
- [31] L. Yu *et al.*, "Monolithically integrated amplified feedback lasers for high-quality microwave and broadband chaos generation," *J. Lightw. Technol.*, vol. 32, no. 20, pp. 3595–3601, Oct. 2014.
- [32] D. Tauber and J. E. Bowers, "Dynamics of wide bandwidth semiconductor lasers," *Int. J. High Speed Electron. Syst.*, vol. 8, no. 3, pp. 377–416, Sep. 1997.
- [33] B. R. Cemlyn, M. J. Adams, I. D. Henning, and D. Labukhin, "Detuning boundaries of linear and nonlinear dynamics in a system of coupled lasers," *IEEE J. Sel. Topics Quantum Electron.*, vol. 21, no. 6, pp. 514–521, Nov. 2015.



under optical injection and optical feedback.

Kevin Schires received the Diplôme d'Ingénieur degree, specializing in signal processing and telecommunications, from the École Supérieure d'Ingénieurs en Électronique et Électrotechnique, Paris, France, and the Ph.D. degree in semiconductor electronics from the University of Essex, Colchester, U.K. He is currently holding a postdoctoral position in the Communications and Electronic Department, Telecom Paristech (former École Nationale Supérieure des Télécommunications) focused on the study of the dynamics of novel semiconductor laser sources



uniform circular array configurations to differentiate between interfering signals and a particular signal of interest. She joined the Ph.D. program at TELECOM Paris Tech in September 2015. Her thesis is focused on advanced laser diodes using new materials in particular those with III–V on silicon, nonlinear dynamics and optical chaos in semiconductor laser systems. She was with the US Army RDECOM Armament Research, Development, and Engineering Center where she served as a Project Officer in the Acoustic and Networked Sensor Division with specific program responsibility in the development of advanced acoustic sensors. She has a strong foundation in systems engineering and extensive experience in defense acquisition, program management, and life cycle support.

Sandra Gomez received the Bachelor's and Master's degrees in electrical engineering from Stevens Institute of Technology, Hoboken, NJ, USA, with a concentration in digital signal processing (DSP). She is currently the Technical Director of the International Technology Center, France, part of the US Army Research, Development, and Engineering Command (RDECOM) Forward Element Center Atlantic, Paris, France. She previously studied acoustic source localization and the tradeoffs of conventional and adaptive beamforming techniques using different

Antonin Gallet received the Master's degree of science from Ecole Normale supérieure de Cachan, Cachan, France, and the Master's degree of engineering from Institut d'optique, Palaiseau, France, in 2015. He started the Ph.D. research with III–V Lab, Palaiseau, France, and Télécom Paristech, Paris, France, in December 2015 to work on III–V/SOI lasers.

615
616
617
618
619
620
621
622
623
624
625
626
627
628
629
630
631
632
633
634



Guang-Hua Duan (S'88–M'90–SM'01) received the Doctorate degree in applied physics from the École Nationale Supérieure des Télécommunications (Telecom ParisTech), Paris, France, in 1991. He was habilitated to direct researches by Université de Paris-Sud in 1995. He is currently the Leader of the research team Silicon Photonics within III–V Lab, which is a joint laboratory of Nokia, Thales, and CEA Leti, and also the Head of the Research Department Heterogeneous integration of III–V on silicon within Nokia Bell Labs. He is also a Guest Professor in Ecole

Supérieure d'Électricité, and École Supérieure d'Optique, giving lectures in the fields of electromagnetism, optoelectronics, and laser physics. Previously, he was an Assistant, then an Associate Professor at Télécom-ParisTech from 1992 to 2000. He was with the University of Maryland as a Visiting Associate Professor from 1998 to 1999. He joined Opto+, Alcatel Research & Innovation Center in Marcoussis in October 2000. He is an author or coauthor of more than 100 journal papers, 250 conference papers, 30 patents, and a contributor to 4 book chapters.



Frédéric Grillot was born in Versailles, France, on August 22, 1974. He received the M.Sc. degree from the University of Dijon, Dijon, France, in 1999, and the Ph.D. degree from the University of Besançon, Besançon, France, in 2003. His doctoral research activities were conducted within the Optical Component Research Department, Alcatel-Lucent, working on the effects of the optical feedback in semiconductor lasers, and the impact this phenomenon has on optical communication systems. From 2003 to 2004, he was with the Institut d'Électronique Fondamentale

(University Paris-Sud) where he focused on integrated optics modeling and on Si-based passive devices for optical interconnects. From September 2004 to September 2012, he was with the Institut National des Sciences Appliquées as an Assistant Professor. From 2008 to 2009, he was also a Visiting Professor at the University of New-Mexico, Albuquerque, NM, USA, leading research in optoelectronics at the Center for High Technology Materials. Since October 2012, he has been working with Telecom Paristech (alias École Nationale Supérieure des Télécommunications), Paris, France, where he became an Associate Professor then a Full Professor in January 2017. Since August 2015, he has also been serving as a Research Professor at the University of New-Mexico. He is the author or coauthor of 77 journal papers, 1 book, 3 book chapters, and more than 170 contributions in international conferences and workshops. His current research interests include advanced quantum confined devices using new materials such as quantum dots and dashes, light emitters based on intersubband transitions, nonlinear dynamics and optical chaos in semiconductor lasers systems, as well as microwave and silicon photonics applications including photonic clocks and photonic analog-to-digital converters. He is an Associate Editor for *Optics Express*, a Senior Member of the SPIE and the IEEE Photonics Society, as well as a Member of the OSA.

635
636
637
638
639
640
641
642
643
644
645
646
647
648
649
650
651
652
653
654
655
656
657
658
659
660
661
662
663
664
665

IEEE PREPRINT

NOTICES

- 667 • Author: If you have not completed your electronic copyright form (ECF) and payment option please return to Scholar One
668 “Transfer Center.” In the Transfer Center you will click on “Manuscripts with Decisions” link. You will see your article details
669 and under the “Actions” column click “Transfer Copyright.” From the ECF it will direct you to the payment portal to select
670 your payment options and then return to ECF for copyright submission.
- 671 • Author: Please be aware that authors are required to pay overlength page charges \$220 per page if the paper is longer than 8
672 pages for Contributions and +12 pages for Invited Papers. If you cannot pay any or all of these charges please let us know.
- 673 • Author: This pdf contains 2 proofs. The first half is the version that will appear on Xplore. The second half is the version that
674 will appear in print. If you have any figures to print in color, they will be in color in both proofs.
- 675 • Author: The option to publish your paper as Open Access expires when the paper is fully published on Xplore. Only papers
676 published in “Early Access” may be changed to Open Access.

QUERIES

- 678 Q1. Author: If you have not completed your electronic copyright form (ECF) and payment option please return to Scholar One
679 “Transfer Center”. In the Transfer Center you will click on “Manuscripts with Decisions” link. You will see your article
680 details and under the “Actions” column click “Transfer Copyright”. From the ECF it will direct you to the payment portal to
681 select your payment options and then return to ECF for copyright submission.

Passive Chaos Bandwidth Enhancement Under Dual-Optical Feedback with Hybrid III–V/Si DFB Laser

Kevin Schires, Sandra Gomez, Antonin Gallet, Guang-Hua Duan, *Senior Member, IEEE*, and Frédéric Grillot

Abstract—The chaotic dynamics of a DFB laser are studied experimentally under a combination of short and long feedbacks. Chaos bandwidth enhancement is demonstrated using a hybrid III–V/Si DFB laser with a large relaxation oscillation frequency (ROF) of 14 GHz. The impact of short feedback on the ROF is studied and an increase of 2 GHz is observed. Under long feedback, the route to chaos of the device and its dependence on the short feedback dynamics are studied. The short feedback allows tuning the chaotic dynamics obtained under long feedback, and the increase of the ROF translates into an enhancement of the chaos bandwidth to above 16 GHz. This configuration can allow generation of wideband chaos using a single laser source in a photonic integrated circuit.

Index Terms—III–V materials, nonlinear dynamics, optical feedback, silicon photonics, secure communications.

I. INTRODUCTION

SILICON photonics offer tight integration of a variety of active and passive optical and electrical components, and gained so much interest in the last decade that it is now considered one of the most promising technology for optical applications [1], [2]. Building on the mature fabrication techniques first developed for microelectronics allows creating photonic integrated circuits (PICs) with a high density of optical components, in high volumes and at low costs. Academic and industrial efforts led to the development of novel technical solutions for a variety of domains including sensing, measurement instrumentation, optical signal processing and telecommunications

Manuscript received February 7, 2017; revised March 30, 2017 and June 29, 2017; accepted June 30, 2017. This work was supported by the European Union Horizon 2020 Programme under the PICs4All Project (<http://www.pics4all.jeppix.eu>). (Corresponding author: Kevin Schires.)

K. Schires and S. Gomez are with Télécom ParisTech, Université Paris-Saclay, Paris 75634, France (e-mail: schires@enst.fr; sandra.gomez@telecom-paristech.fr).

A. Gallet is with Télécom ParisTech, Université Paris-Saclay, Paris 75634, France, and also with the III–V Lab, Joint Laboratory of Nokia Bell Labs, Thales Research and Technology, and CEA-Leti, Fresnel 91767, France (e-mail: antonin.gallet@3-5lab.fr).

G.-H. Duan are with the III–V Lab, Joint Laboratory of Nokia Bell Labs, Thales Research and Technology, and CEA-Leti, Fresnel 91767, France (e-mail: guanghua.duan@3-5lab.fr).

F. Grillot is with Télécom ParisTech, Université Paris-Saclay, Paris 75634, France, and also with the Center for High Technology Materials, University of New Mexico, Albuquerque, NM 87106-4343 USA (e-mail: grillot@telecom-paristech.fr).

Color versions of one or more of the figures in this paper are available online at <http://ieeexplore.ieee.org>.

Digital Object Identifier 10.1109/JSTQE.2017.2732830

[3], [4]. Recent advances in data centers and informatics [5] reveal how photonic integration will become increasingly used for data transmission, either inside a chip or for short-access and long-haul telecommunications networks [6], [7].

Each discrete component used in electro-optical devices had to be redesigned for integration on Si, and a number of research works allowed developing novel integrated modulators, photodetectors, isolators, polarization controllers, amplifiers, as well as novel laser sources [8]. As laser cavities had to be adapted for integration into PICs, novel fabrication techniques were derived for the growth of the active material, and novel designs of the resonant cavity were proposed [9]–[12]. The active III–V material is generally not grown directly on a Si substrate but rather wafer bonded onto a Si waveguide: lattice mismatches between III–V compounds and Si as well as different thermal expansion lead to dislocation in Quantum Well (QW) materials and to poor device reliability. Novel Quantum Dot (QD) laser sources grown directly on Si have recently been reported [13], [14]: unlike QW materials, the localization of carriers in QDs make these less sensitive to defects. Complex laser cavities for single and multimode laser sources have been proposed [15], but such designs were shown to suffer from stability issues due to internal feedback sources [16] and a simpler DFB structure is studied in this work.

Multisection lasers have been demonstrated on PICs, and devices with an integrated external feedback cavity for use as chaotic emitters are of interest for both academic and industrial research [17]–[19]. PICs creating an external cavity with a phase section are important for research purposes as they allow study of the behavior of lasers under optical feedback with short cavities of controllable length, thus giving new insights into laser dynamics [20], [21]. Under optical feedback of increasing strength, the laser’s relaxation oscillations become excited and lead to chaotic oscillation of the laser output [22]. PICs containing lasers with and external optical feedback cavity are thus very important for practical applications, as they allow the use of chaotic emitters in communication networks without imposing volume constraints for integration into existing emitter and receiver modules.

Two major applications of chaotic emitters in communication networks are random number generation and most importantly secure communications [23]. Chaotic communications rely on hiding data within a broad chaotic spectrum at the emitter level, and the data is recovered in the receiver. The bandwidth of the

76 amplified feedback should thus be maximized to increase trans-
 77 mission rates while keeping the data secure, and several schemes
 78 were proposed to obtain large chaos bandwidth, defined as the
 79 frequency under which 80% of the RF power is found [24]. Pas-
 80 sive enhancement of the chaos bandwidth was proposed using
 81 phase-conjugate feedback and a high-reflectivity mirror [25].
 82 Active solutions using optical injection from two laser sources
 83 in addition to optical feedback demonstrated chaos bandwidths
 84 as high as 32 GHz [26].

85 Another way of generating broad chaos is to increase the
 86 relaxation oscillation frequency (ROF) of the laser source.
 87 Under optical feedback, the generated chaotic spectra scale
 88 with the relaxation frequency of the laser, as chaotic dynamics
 89 build up from enhanced relaxation oscillations. In addition, the
 90 ROF can be tuned using optical feedback, depending on the
 91 feedback phase and strength [22], [27], [28], and that dynamics
 92 can be generated by tailoring the feedback and controlling its
 93 phase [29]. It was demonstrated that PICs with an integrated
 94 amplified external cavity with a phase section allowed forcing
 95 self-pulsations in the laser at a frequency tuneable to above
 96 40 GHz [30], [31].

97 In this article, we study the enhancement of the bandwidth of
 98 chaotic dynamics using a combination of two passive cavities of
 99 different scales. Chaos bandwidth enhancement is demonstrated
 100 using a hybrid III-V/Si QW DFB laser in order to prove appli-
 101 cations to PICs. As the optical cavities are created in a fibered
 102 setup and not within the chip, only low feedback strengths are
 103 achieved. This study shows for the first time the evolution of
 104 the dynamics of a hybrid III-V/Si DFB laser with the strength
 105 of a long feedback or the phase of a short feedback, and combi-
 106 nations of the two. In Section I, the device is presented and
 107 characterized, and the impact of internal reflections on laser
 108 operation is discussed. The free-running laser exhibits high re-
 109 laxation oscillations of 14 GHz which make it ideal for this study
 110 as large ROF simplifies the access to wide chaos bandwidths.
 111 The route to chaos of the hybrid laser under long feedback is
 112 studied in Section III, and compared with that of a commercial
 113 III-V DFB laser, showing similar behaviors between the two
 114 types of laser despite significant differences in their structures.
 115 In Section IV, the laser is subject to a short feedback cavity
 116 which allows increasing its ROF by 2 GHz. In Section V, the
 117 laser is subject to both feedback cavities, and the chaos band-
 118 width is found to be enhanced in the same fashion as the ROF.
 119 The chaos bandwidth is increased by up to 13% and reaches a
 120 maximum of 16.4 GHz, showing that this combination of two
 121 feedbacks allows controlling the bandwidth and characteristics
 122 of the generated chaos despite the very low feedback strength
 123 allowed by the setup. Such passive chaos bandwidth enhance-
 124 ment can be applied to standard III-V DFB lasers, and the setup
 125 is transposable to a PIC constituted of the laser and two cavities
 126 with optional phase sections, allowing wide chaos generation
 127 with low power consumption.

128 II. EXPERIMENTAL APPARATUS

129 A. Device Studied

130 Fig. 1 presents a schema of the DFB structure studied. The
 131 1 mm-long hybrid III-V Silicon-on-Insulator (SOI) device is

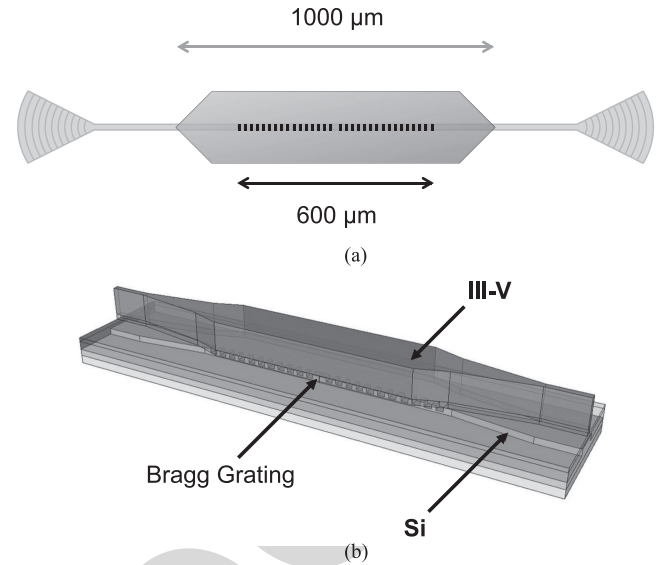


Fig. 1. (a) Schematic and (b) structure of the device studied, showing the Si waveguide (yellow) and the III-V material (green). The vertical couplers are represented in (a) at both extremities of the Si waveguide.

132 fabricated using a III-V QW active medium bonded on top of
 133 the processed silicon waveguide, and constituted of a DFB laser
 134 with tapers on each side [15]. To ensure single-mode operation,
 135 a 50 nm-deep and 600 μm -long Bragg grating with a quarter-
 136 wavelength phase shift in the center is etched on the silicon
 137 waveguide. The strength of the grating is chosen such that the
 138 product κL_{bragg} is of a few units, and the period of the grating
 139 is of 240 nm. The light is coupled from the Si waveguide to the
 140 III-V material with adiabatic tapers, and outcoupled using Verti-
 141 cal Bragg Gratings (VBG) on both side of the device. The VBG
 142 couples the light out of the laser with an angle of 80° from the
 143 waveguide, and light was thus coupled vertically using a fiber
 144 positioned above the laser, with a 10° angle from the normal
 145 to the lasers surface. The VBG were only necessary for testing
 146 purposes, in order to characterize several unprocessed devices
 147 on the same bar, and in a PIC they would not be positioned after
 148 the laser. They however affected our study in two ways: first via
 149 their transmission losses of approximately 7 dB, which will be
 150 discussed later, and secondly by their parasitic reflectivity (be-
 151 low -23 dB) which affected laser operation when biased high
 152 above threshold.

153 B. Characterisation

154 Fig. 2(a) presents the evolution of the power coupled into an
 155 anti-reflection (AR)-coated lens-ended fiber with the bias cur-
 156 rent. All measurements presented in this paper were performed
 157 at 20°C . Around the threshold of about 45 mA, the laser ex-
 158 hibits slight competition between two modes which translates
 159 into a kink in the curve. Between 50 and 150 mA, very stable
 160 single-mode operation is observed with a side-mode suppression
 161 ratio above 50 dB. Above 4 times threshold, the laser exhibited
 162 power drops which were also observed on the other lasers of
 163 the same bar, but differed from device to device. Such behavior
 164 hints that parasitic reflections are present within the devices:
 165 the vertical couplers and tapers create reflections which only

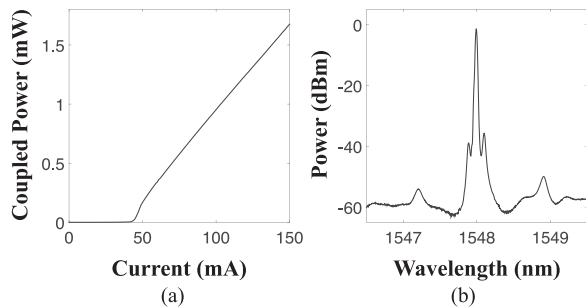


Fig. 2. (a) Evolution of the power coupled using an AR-coated lensed fiber with the pump current. (b) Optical spectrum at a bias current of 140 mA.

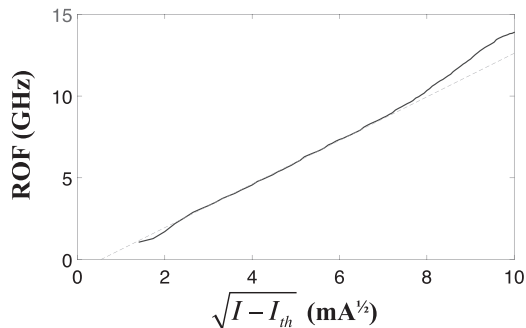


Fig. 3. Evolution of the ROF with the square root of the current overdrive above threshold.

166 seem to affect the laser far above threshold through variations
 167 of the optical power or changes in the ROF, as will be discussed
 168 next. As the amount of parasitic reflections varies from device
 169 to device, different sorts of power variation would indeed be
 170 expected between the different lasers. Fig. 2(b) presents the
 171 spectrum of the laser at 140 mA, showing the well-suppressed
 172 side-modes as well as sidebands characteristic of relaxation oscil-
 173 lations. These spectra were measured using a Yenista OSA20
 174 optical spectrum analyzer with a 20 pm resolution, and these
 175 sidebands could be measured thanks to the rather high value of
 176 the ROF.

177 Fig. 3 presents the evolution of the ROF as a function of the
 178 square root of the current overdrive above threshold. It can
 179 be noted that very high frequencies are observed as the ROF
 180 reaches 14 GHz at 150 mA. Usually, due to gain compression,
 181 the power evolves in a sublinear fashion with increasing bias
 182 current, and the squared ROF follows the same trend. Here, it
 183 can be seen that the ROF rather evolves in the opposite way as
 184 it gradually increases above the linear fitting shown as a dashed
 185 line.

186 We believe that these high values of ROF stem from the use
 187 of Aluminium in the III-V compound forming the QW [32], but
 188 also from the aforementioned internal feedback. Under optical
 189 feedback, the ROF can oscillate around its free-running value
 190 depending on the feedback strength and delay [22]. Here, the
 191 internal feedback conditions thus allow a small enhancement of
 192 the ROF for some bias currents, showing an effect of parasitic
 193 feedback very different from the detrimental impact it can have
 194 further above threshold.

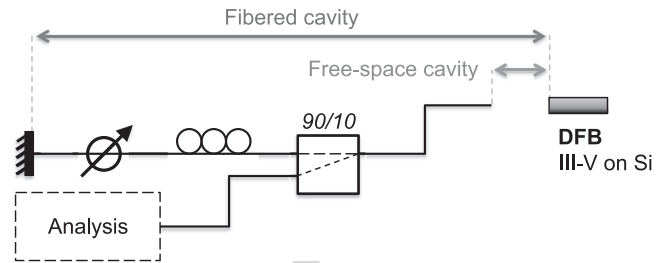


Fig. 4. Experimental setup allowing combination of short and long feedback.

C. Experimental Setup

195

196 Fig. 4 presents the experimental setup used for the following
 197 measurements [16]. The DFB is kept at a bias current of 146 mA
 198 and at 20 °C. The light of the DFB laser is coupled using either an
 199 AR-coated lensed fiber or a cleaved uncoated one. The cleaved
 200 fiber allows creating a short free-space feedback cavity [33] of
 201 the order of 100 μm , re-injecting about 3% of the light back
 202 into the device with a time delay below 1 ps. On the other hand,
 203 the lens-ended fiber minimizes such reflections and only allows
 204 light from the setup to be re-injected into the device. In the
 205 fiberized setup, a 90/10 splitter is used to create a feedback
 206 path consisting of a polarization controller and a Yonista Back-
 207 Reflector (BKR) module, equivalent to a mirror with variable
 208 losses. This long fibered cavity measures approximately 7 m
 209 and allows re-injecting at most 8% of the light into the device.
 210 Note that due to the transmission losses of the vertical couplers,
 211 a difference must be made between the light re-injected into
 212 the component and the light that reaches the laser cavity. The
 213 maximum feedback strengths considering the light that reaches
 214 the laser cavity are thus of 0.1% and 0.3% for the short and long
 215 cavities, respectively.

216 Using either fiber and controlling the attenuation of the long
 217 feedback path allows studying the laser into the following four
 218 situations: free-running with only parasitic reflections from
 219 the setup, under short (free-space) feedback only, under long
 220 (fibered) feedback only, and under a combination of both feed-
 221 backs. For the short feedback, while the feedback strength is
 222 fixed by the refractive index of the fiber, the phase can be tuned
 223 using a piezoelectric actuator allowing gradually moving the
 224 fiber towards or away from the device. Concerning the long
 225 feedback, while the feedback phase can be changed the same
 226 way it does not impact laser behavior given the large external
 227 cavity length. Feedback strength can however be tuned by
 228 changing the attenuation of the BKR.

III. LONG FEEDBACK

229

230 To assess the potential of such hybrid lasers as chaotic emit-
 231 ters, we first study the route to chaos that the devices follow
 232 under long feedback. The cavity used here is too long to repre-
 233 sent the external cavity that would be integrated in a PIC, but it
 234 allows pushing the laser into chaotic operation where the phase
 235 of the long feedback has little impact on the dynamics. This
 236 will later allow us to dissociate the effect of the short and long
 237 feedbacks when combined together, as we can consider that the
 238 feedback phase will only affect the dynamics induced by the

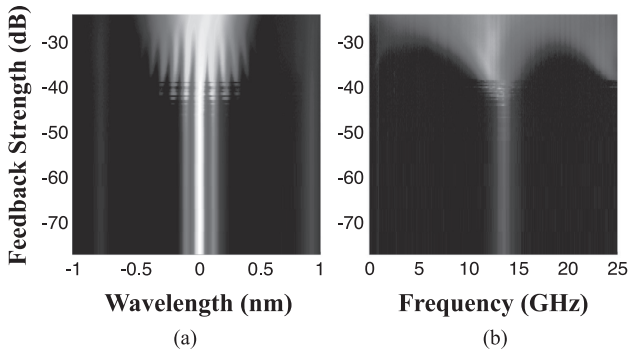


Fig. 5. Evolution of the (a) optical and (b) RF spectra with long feedback strength, using a lens-ended fiber.

short feedback. Fig. 5 presents the evolution of the optical and RF spectra with the long feedback strength, using the lensed fiber. The measurements performed with the lensed fiber have very little dependence on the position of the fiber and thus the feedback phase, as it will be shown later in the case of the free-running laser. Routes to chaos under long feedback were thus found to be identical for different positions of the fiber.

The route observed is typical of a DFB laser under long optical feedback despite major differences in the device structures: first of all, the hybrid DFB is constituted of two evanescently coupled waveguides, one passive and one active, unlike the standard III-V DFB. In addition, in the hybrid device the tapered regions on each side of the DFB structure may slightly amplify the light fed back into the laser, or even act as source of internal reflections [16]. The proposed chaos bandwidth enhancement method could also be applied to a standard III-V DFB, for which higher feedback strengths could be achieved. Demonstrating the changes in ROF and bandwidth in the case of hybrid lasers is however interesting, as it shows that the complexity of the lasers used in PICs does not necessarily affect their behavior under optical feedback.

For very low feedback strengths, the ROF can be seen at 14 GHz in the RF spectrum. Around -43 dB of feedback strength, temporally unstable periodic oscillations start to appear, and stabilize above -40 dB. These correspond to an excitation of relaxation oscillations that turn into chaotic dynamics above -30 dB of feedback strength. Under maximum feedback strength, the bandwidth of the chaotic spectra is of 14.5 GHz.

Fig. 6 allows comparing the route to chaos of this hybrid DFB laser with that of a commercial Nokia III-V DFB laser. The laser is operated a three times its threshold where it has a ROF of 8 GHz. The routes appear to be very similar. Along the feedback strength axis, the routes appear to be shifted by 6 dB as the III-V DFB reaches chaotic operation for only -36 dB of feedback strength. Note that in the case of the III-V laser, higher feedback strengths were achievable with the same setup as there were no extra losses between the fiber and the laser cavity. It can thus be seen that with the hybrid DFB we are only able to merely enter the chaotic regime, and that much broader spectra could be observed for stronger feedback. Along the wavelength axis, broader spectra are observed for the hybrid DFB in the region of periodic oscillations, as the base frequency of these oscillations

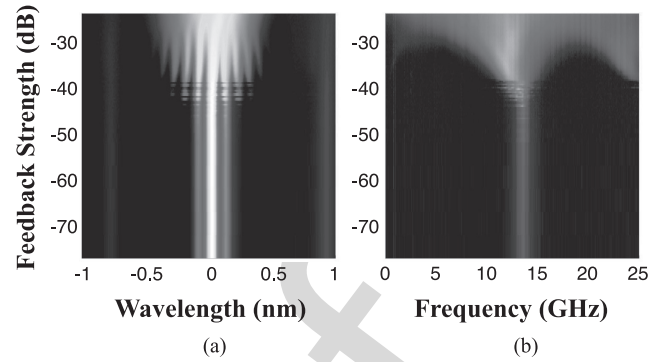


Fig. 6. Evolution of the optical spectra of a (a) III-V and (b) III-V/Si DFB laser with long feedback strength, using a lens-ended fiber.

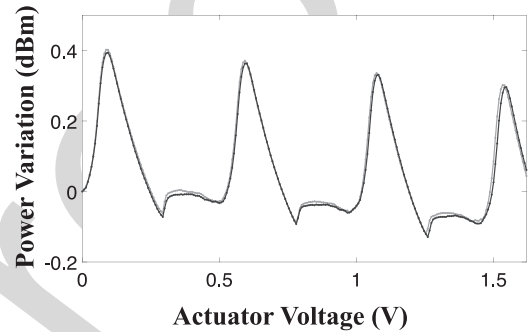


Fig. 7. Variation of the power coupled with the cleaved fiber as a function of the voltage applied to the piezoelectric actuator. Two measurements for different fiber positions are presented in black and grey.

is the ROF, and we expect that the spectra observed for the III-V DFB could be obtained for the hybrid one, broadened by a factor close to the ratio between the two ROFs.

IV. SHORT FEEDBACK

Using the cleaved fiber and setting the long feedback strength to its minimum of -79 dB allows studying the DFB under short feedback only. Fig. 7 presents the variation of the coupled power as a function of the voltage applied to the piezoelectric actuator. As the coupling is only optimized for a voltage of 0 V, the power fades as the fiber is moved away from the device and the figure appears skewed. A clear periodicity can however be observed in the evolution of the power, as we are varying the phase of the short feedback. For convenience, we choose as beginning of each period the main peaks and consider that between each peak, the phase is varied from 0 to 2π . Note that this does not represent the absolute phase of the feedback, but only a representation of the phase shift within a period.

Such variation of the output power under optical feedback corresponds to the effect of a medium feedback strength and usually exhibits bistability when the mirror is moved one way or the other [22]. Fig. 8 presents a comparison between the evolution of the power and spectrum when the fiber is moved in both directions, as well as reference measurements performed with the lensed fiber. The reference measurements shows the weak impact of all parasitic reflections from the setup, and shows that the cavity created by the cleaved fiber is mainly responsible

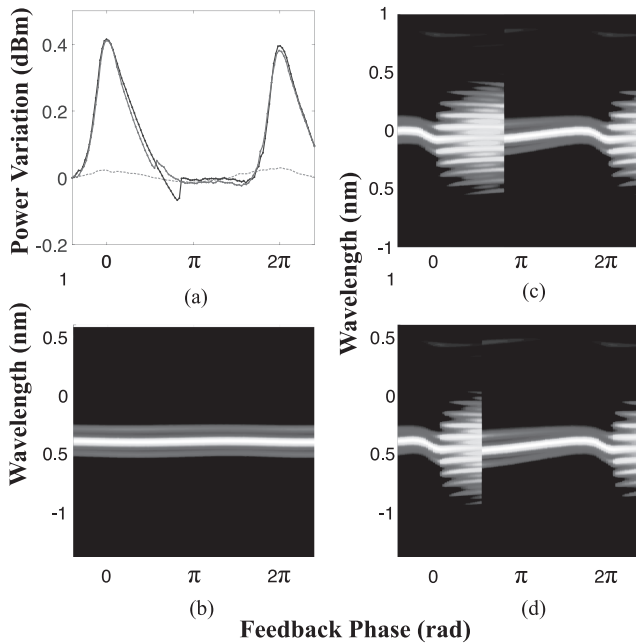


Fig. 8. (a) Variation of the power coupled with the cleaved fiber within one period when the fiber is moved away (black) or towards (red) the laser. The grey dashed line represents the power coupled when using the lensed fiber. (b) Evolution of the optical spectrum when using the lensed fiber. (c) and (d) Show the evolution of the optical spectrum when moving the fiber away or towards the laser, respectively.

307 for the power variation presented above. In Fig. 8(a) the gray
 308 dashed line shows that the power is oscillating sinusoidally
 309 with a low amplitude, which corresponds to the impact of weak
 310 feedback. Fig. 8(b) shows that the wavelength varies in a similar
 311 fashion. This confirms that any other variation of the power or
 312 wavelength is only due to the feedback created by the cleaved
 313 fiber. Fig. 8(a) also reveals a slight bistability in the evolution
 314 of the power, as the kinks observed after the peak occur for
 315 a phase shift of 0.3π for one direction and 0.4π for the other.
 316 While the bistability in the output power is negligible, it makes
 317 a significant difference in the optical spectrum. Note that all
 318 spectrum maps presented in this work are plotted in dBm, with
 319 a logarithmic color scale.

320 Fig. 8(c) reveals that during each periods, the laser exhibits
 321 periodic dynamics between phases of 0 and 0.4π , with period
 322 doubling above 0.2π . When the kink occurs in the optical power,
 323 the laser suddenly stabilises, and it can be seen from the side-
 324 bands that the ROF changes with the phase. Fig. 8(d) shows that
 325 the same behaviour is observed when the fiber is moved in the
 326 opposite direction, thus leading to a wider region of stability.
 327 This wider region is of importance for this study as it appears
 328 that the largest ROFs are achieved within the bistability window
 329 when the laser is stable, as this is where the mode's sidebands
 330 appear to be the farthest apart.

331 Fig. 9 shows the evolution of the optical and RF spectra of the
 332 DFB as the fiber is moved towards the laser, at a shorter distance.
 333 In order to clearly see the peak of the relaxation oscillations in
 334 the RF spectra, an EDFA set to a fixed output power of 10 dBm
 335 was used to amplify the light before detection. A photodetector
 336 with a bandwidth of 30 GHz and a Rohde & Schwartz FSP

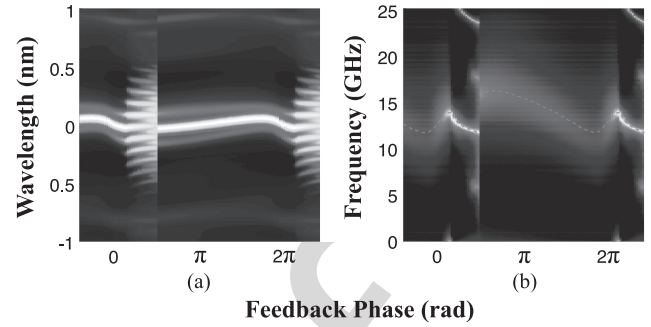


Fig. 9. Evolution of the (a) optical and (b) RF spectra within one period. The green dashed line shows the evolution of the ROF.

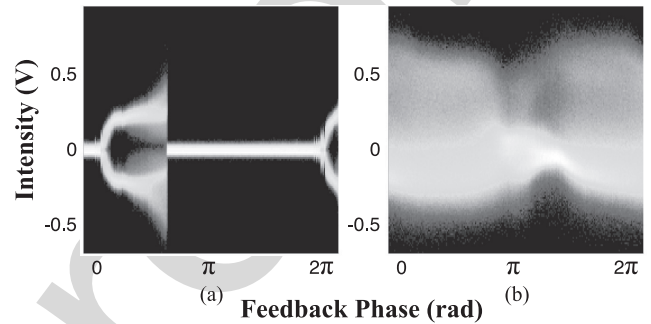


Fig. 10. Bifurcation diagrams as a function of the short feedback phase under (a) minimum and (b) maximum long feedback strength.

40 GHz electrical spectrum analyzer were used to perform the
 337 spectrum measurements. A slightly larger stability region is
 338 obtained, and the RF spectra show that within one period, the
 339 ROF varies between a minimum of 11 GHz and a maximum of
 340 16 GHz, thus allowing reaching frequencies 2 GHz higher than
 341 the free-running ROF.
 342

V. COMBINATION OF FEEDBACKS 343

344 Under long feedback only, the hybrid DFB exhibits a classic
 345 route to chaos where chaotic dynamics are obtained from the
 346 excitation of relaxation oscillations. Under short feedback only,
 347 it is possible to tune the value of the ROF while keeping the laser
 348 into stable operation. Combining both feedbacks will allow us to
 349 study whether the enhancement of the ROF under short feedback
 350 can be used to generate broader chaos by first tailoring the ROF
 351 and then exciting relaxation oscillations into chaotic ones. In
 352 this section, the laser is thus subjected to a combination of short
 353 and long feedbacks by using the cleaved fiber and varying the
 354 long feedback strength.

355 Fig. 10 presents the bifurcation diagrams of the dynamics as
 356 a function of the phase of the short feedback, under minimum
 357 and maximum long feedback strengths. Under minimum long
 358 feedback strength, the diagram clearly shows the apparition of
 359 the periodic oscillations and the sudden transition from oscil-
 360 lating to stable operation. Under maximum feedback, it can be
 361 seen that the chaotic signal changes significantly with the short
 362 feedback phase.

363 Fig. 11 presents the evolution of optical and RF spectra with
 364 the position of the cleaved fiber for four levels of long feedback

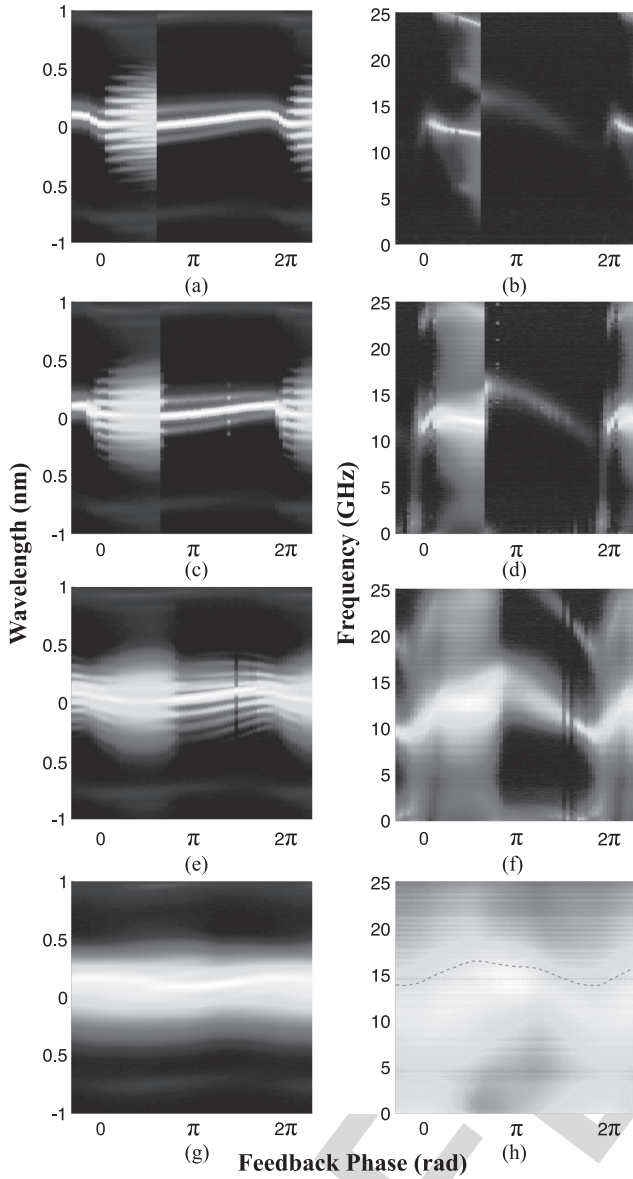


Fig. 11. Evolution of optical (left) and RF (right) spectra with the position of the cleaved fiber for long feedback strengths of (a), (b) -79 dB, (c), (d) -42 dB, (e), (f) -36 dB and (g), (h) -26 dB. In (h) the black line shows the chaos bandwidth under long feedback only, and the green dashed line shows the evolution of chaos bandwidth with the phase of the short feedback.

365 strength: the minimum of -79 dB, -42 dB, -36 dB and the
 366 maximum of -26 dB. No optical amplification was used for
 367 the RF spectrum measurements. The route towards chaos under
 368 long feedback clearly changes with the short feedback phase, as
 369 periodic dynamics appear for different long feedback strengths
 370 at the different positions of the cleaved fiber. Regions where
 371 periodic oscillations occur under short feedback alone appear
 372 to enter chaotic operation first. The sharp transition between
 373 oscillating and stable operation gradually disappears as the long
 374 feedback strength is increased. In a similar way as in Figs. 5
 375 and 6, some points exhibit temporally unstable dynamics for
 376 feedback phases between 1.3π and 1.5π and feedback strengths
 377 of -42 and -36 , which can be seen as a disappearance of the

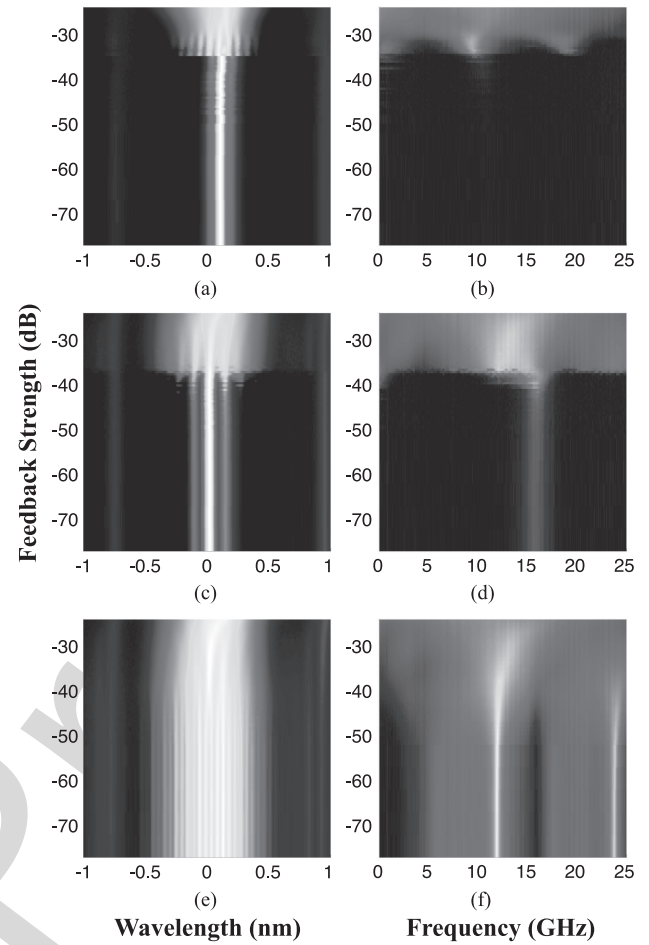


Fig. 12. Evolution of the optical (left) and RF (right) spectra with the long feedback strength for three positions of the cleaved fiber. (a) and (b) correspond to a feedback phase of 1.9π (minimum ROF, stable). (c) and (d) correspond to a feedback phase of 0.3π (maximum ROF, stable). (e) and (f) correspond to a feedback phase of 0.25π (strongest oscillations).

dynamics for some isolated feedback phases. It is interesting
 378 to observe that, as the long feedback strength is increased, the
 379 wavelength of the spectrum peak oscillates in a more and more
 380 sinusoidal fashion, such that no bistability was observed under
 381 maximum long feedback strength.
 382

The long feedback strength necessary to reach chaotic operation
 383 seems to depend on the short feedback phase, and it can be
 384 seen in Fig. 11(g) and (h) that the width of the chaotic spectrum
 385 varies with the feedback phase too. In Fig. 11(h), the super-
 386 imposed green dashed line shows the evolution of the chaos
 387 bandwidth with the short feedback phase. The black dotted line
 388 shows as a reference the bandwidth of the chaos measured under
 389 maximum long feedback only, corresponding to the spectrum
 390 under maximum long feedback strength in Fig. 5(b). With the
 391 addition of short feedback, the chaos bandwidth oscillates be-
 392 tween 13.7 and 16.4 GHz by following very closely the evolu-
 393 tion of the ROF in Fig. 9(b). Minimum and maximum chaos
 394 bandwidth are indeed respectively found close to the feedback
 395 phases where minimum and maximum ROF are observed in the
 396 absence of long feedback.
 397

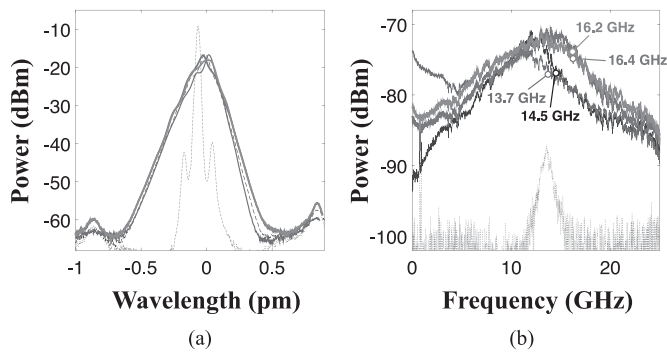


Fig. 13. Optical (left) and RF (right) spectra under maximum long feedback and their bandwidth, the dashed lines showing the free-running spectra as reference. The black curve corresponds to maximum long feedback alone. The blue (resp. red) curve corresponds to both feedbacks with minimum (maximum) ROF. The green curve corresponds to both feedback with strongest periodic oscillations.

Three specific routes to chaos are thus of interest: those where short feedback does not destabilize the laser but induces either a reduction of the ROF to its minimum value of 11 GHz (phase of 1.9π) or an increase to its maximum value of 16 GHz (phase of 0.3π), and one where short feedback induces the strongest periodic oscillations (phase of 0.25π). Fig. 12 presents these three routes. In the first two routes, the laser remains stable until slightly higher feedback strengths than compared to Fig. 5(a). The window where periodic oscillations are observed is however very narrow, as chaos appears around the same feedback strength of about -30 dB. In the last route, chaotic dynamics seem to appear for a lower long feedback strength of -38 dB, but under maximum long feedback the end of the route appears similar to that in Fig. 12(d). This is however not surprising given that the last two routes are measured for short feedback phases that are rather close, and that no discontinuity can be seen in Fig. 11(g) and (h) between these phases.

The optical and RF spectra obtained under maximum long feedback for these three operating conditions are shown in Fig. 13, along with the free-running spectra and the chaotic ones obtained under maximum long feedback alone. Fig. 13(b) shows that the chaotic spectrum obtained for a feedback phase of 1.9π leads to the minimum bandwidth of 13.7 GHz observed in Fig. 11(h). Both the other routes lead to a bandwidth of 16.2 GHz, despite slight differences in the chaotic spectra.

VI. CONCLUSION

A combination of long and short feedback are used to respectively generate chaotic dynamics in a DFB laser and tune the chaos bandwidth. The dynamics of a hybrid III-V/Si DFB laser were studied under such combination of feedbacks to show the possibility to achieve passive chaos bandwidth enhancement in PICs. The routes of the dynamics are extensively characterized by varying the phase of the short feedback and strength of the long one. Owing to the large ROF of the free-running laser, chaotic dynamics with a bandwidth of 14.5 GHz can be generated using a long external feedback cavity. The route to chaos

appears to be very similar to that of a standard commercial III-V DFBs, but due to the transmission losses of the device's vertical couplers, maximum feedback strengths of only 0.3% were achievable. The impact of a short external cavity on the laser dynamics revealed a variation of the ROF of 5 GHz, with a maximum value of 16 GHz. When combining short and long feedbacks, this 2 GHz increase of the ROF translates into a similar increase of the chaos bandwidth, which reaches 16.4 GHz.

The tuneability of the chaotic dynamics and of their bandwidth is of interest for applications requiring random number generation, or broad chaos generation. With feedback cavities integrated into a Si waveguide along with a phase section, higher feedback strengths would be achievable for both short and long feedbacks. Chaotic spectra much wider than those reported in this work could thus be obtained using a single component and passive optical cavities with optional phase sections. This would be of prime importance for the development of low-consumption integrated chaotic transmitters and receivers for secure communications.

As the wide bandwidth relies primarily on the large ROF of the laser, the design of the device is extremely important, and for these applications QW sources may be more appealing than QD sources as QW lasers generally exhibit much higher ROFs than QD ones. In the case of application in a Si PIC, the design of the Si waveguides would be very important too, as all the possible sources of reflections within the PIC will affect the dynamics of the laser. In this work, at least two feedback cavities allow pushing the ROF towards the values reported here: the cavity created by the cleaved fiber, but also the internal parasitic sources of feedback which seem to increase the ROF of the free-running laser already. If sources of feedback are inevitable in a PIC, they can thus be designed to potentially enhance the laser's operation instead of hindering it.

Future work will focus on the simulation of single mode III-V and III-V/Si lasers subject to two external cavities in order to attempt to replicate these experimental results. Conditions to maximize the increase of the ROF under short feedback will thus be studied in the presence of several short cavities, in order to reach larger bandwidth enhancements. It will also be possible to determine which absolute feedback phase leads to the wider chaos bandwidth, to see if it is phase-conjugate feedback that leads to the largest enhancement. Finally, the theoretical results should allow identifying the minimum length of the long cavity required to achieve sufficient chaos bandwidth, which will help the design and realization of an integrated wideband chaos generator.

REFERENCES

- [1] D. Thomson *et al.*, "Roadmap on silicon photonics," *J. Opt.*, vol. 18, no. 7, 2016, Art. no. 073003.
- [2] L. Vivien and L. Pavesi, *Handbook of Silicon Photonics*. Boca Raton, FL, USA: CRC Press, Apr. 2013.
- [3] G. Roelkens *et al.*, "Silicon-based heterogeneous photonic integrated circuits for the mid-infrared," *Opt. Mater. Express*, vol. 3, no. 9, pp. 1523–1536, Sep. 2013.
- [4] A. Rickman, "The commercialization of silicon photonics," *Nature Photon.*, vol. 8, no. 8, pp. 579–582, Aug. 2014.

- [5] C. Sun *et al.*, "Single-chip microprocessor that communicates directly using light," *Nature*, vol. 528, no. 7583, pp. 534–538, Dec. 2015.
- [6] M. Asghari and A. V. Krishnamoorthy, "Silicon photonics: Energy-efficient communication," *Nature Photon.*, vol. 5, no. 5, pp. 268–270, May 2011.
- [7] Y. A. Vlasov, "Silicon CMOS-integrated nano-photonics for computer and data communications beyond 100 g," *IEEE Commun. Mag.*, vol. 50, no. 2, pp. s67–s72, Feb. 2012.
- [8] M. J. R. Heck, "Grating coupler enabled optical isolators and circulators for photonic integrated circuits," *IEEE J. Sel. Topics. Quantum Electron.*, vol. 21, no. 4, pp. 361–369, Jul. 2015.
- [9] A. W. Fang *et al.*, "Electrically pumped hybrid AlGaInAs-silicon evanescent laser," *Opt. Express*, vol. 14, no. 20, pp. 9203–9210, Oct. 2006.
- [10] A. W. Fang *et al.*, "Hybrid silicon evanescent devices," *Mater. Today*, vol. 10, no. 78, pp. 28–35, Jul. 2007.
- [11] G. Roelkens *et al.*, "III-V/Si photonics by die-to-wafer bonding," *Mater. Today*, vol. 10, no. 78, pp. 36–43, Jul. 2007.
- [12] H. Park *et al.*, "Device and integration technology for silicon photonic transmitters," *IEEE J. Sel. Topics. Quantum Electron.*, vol. 17, no. 3, pp. 671–688, May 2011.
- [13] A. Y. Liu *et al.*, "High performance continuous wave 1.3μm quantum dot lasers on silicon," *Appl. Physics Lett.*, vol. 104, no. 4, Jan. 2014, Art. no. 041104.
- [14] S. Chen *et al.*, "Electrically pumped continuous-wave III-V quantum dot lasers on silicon," *Nature Photon.*, vol. 10, no. 5, pp. 307–311, May 2016.
- [15] G. H. Duan *et al.*, "Hybrid III-V on silicon lasers for photonic integrated circuits on silicon," *IEEE J. Sel. Topics. Quantum Electron.*, vol. 20, no. 4, pp. 158–170, Jul. 2014.
- [16] K. Schires *et al.*, "Dynamics of hybrid III-V silicon semiconductor lasers for integrated photonics," *IEEE J. Sel. Topics Quantum Electron.*, vol. 22, no. 6, pp. 43–49, Nov. 2016.
- [17] A. Argyris, M. Hamacher, K. E. Chlouverakis, A. Bogris, and D. Syvridis, "Photonic integrated device for chaos applications in communications," *Physical Rev. Lett.*, vol. 100, no. 19, May 2008, Art. no. 194101.
- [18] A. Argyris, S. Deligiannidis, E. Pikasis, A. Bogris, and D. Syvridis, "Implementation of 140 Gb/s true random bit generator based on a chaotic photonic integrated circuit," *Opt. Express*, vol. 18, no. 18, pp. 18 763–18 768, Aug. 2010.
- [19] R. Takahashi *et al.*, "Fast physical random bit generation with photonic integrated circuits with different external cavity lengths for chaos generation," *Opt. Express*, vol. 22, no. 10, pp. 11 727–11 740, May 2014.
- [20] A. K. Dal Bosco *et al.*, "Cycles of self-pulsations in a photonic integrated circuit," *Physical Rev. E*, vol. 92, no. 6, Dec. 2015, Art. no. 062905.
- [21] A. K. Dal Bosco *et al.*, "Photonic integrated circuits unveil crisis-induced intermittency," *Opt. Express*, vol. 24, no. 19, pp. 22 198–22 209, Sep. 2016.
- [22] J. Ohtsubo, *Semiconductor Lasers: Stability, Instability and Chaos*. New York, NY, USA: Springer-Verlag, 2013.
- [23] A. Argyris *et al.*, "Chaos-based communications at high bit rates using commercial fibre-optic links," *Nature*, vol. 438, no. 7066, pp. 343–346, Nov. 2005.
- [24] H. Someya, I. Oowada, H. Okumura, T. Kida, and A. Uchida, "Synchronization of bandwidth-enhanced chaos in semiconductor lasers with optical feedback and injection," *Opt. Express*, vol. 17, no. 22, pp. 19 536–19 543, Oct. 2009.
- [25] A. Mercier, D. Wolfersberger, and M. Sciamanna, "Improving the chaos bandwidth of a semiconductor laser with phase-conjugate feedback," *Proc. SPIE*, vol. 9892, 2016, Art. no. 98 920G.
- [26] M. Zhang *et al.*, "Generation of broadband chaotic laser using dual-wavelength optically injected Fabry-Perot laser diode with optical feedback," *IEEE Photon. Technol. Lett.*, vol. 23, no. 24, pp. 1872–1874, Dec. 2011.
- [27] D. Lenstra, "Relaxation oscillation dynamics in semiconductor diode lasers with optical feedback," *IEEE Photon. Technol. Lett.*, vol. 25, no. 6, pp. 591–593, Mar. 2013.
- [28] D. D'Agostino, H. P. M. M. Ambrosius, M. K. Smit, and D. Lenstra, "Integrated laser with optical feedback shows suppressed relaxation-oscillation dynamics," *IEEE Photon. Technol. Lett.*, vol. 27, no. 21, pp. 2292–2295, Nov. 2015.
- [29] J. Zhao *et al.*, "Stability of a monolithic integrated filtered-feedback laser," *Opt. Express*, vol. 20, no. 26, pp. B270–B278, Dec. 2012. [Online]. Available: <https://www.osapublishing.org/abstract.cfm?uri=oe-20-26-B270>
- [30] O. Brox *et al.*, "High-frequency pulsations in DFB lasers with amplified feedback," *IEEE J. Quantum Electron.*, vol. 39, no. 11, pp. 1381–1387, Nov. 2003.
- [31] L. Yu *et al.*, "Monolithically integrated amplified feedback lasers for high-quality microwave and broadband chaos generation," *J. Lightw. Technol.*, vol. 32, no. 20, pp. 3595–3601, Oct. 2014.
- [32] D. Tauber and J. E. Bowers, "Dynamics of wide bandwidth semiconductor lasers," *Int. J. High Speed Electron. Syst.*, vol. 8, no. 3, pp. 377–416, Sep. 1997.
- [33] B. R. Cemlyn, M. J. Adams, I. D. Henning, and D. Labukhin, "Detuning boundaries of linear and nonlinear dynamics in a system of coupled lasers," *IEEE J. Sel. Topics Quantum Electron.*, vol. 21, no. 6, pp. 514–521, Nov. 2015.



under optical injection and optical feedback.

Kevin Schires received the Diplôme d'Ingénieur degree, specializing in signal processing and telecommunications, from the École Supérieure d'Ingénieurs en Électronique et Électrotechnique, Paris, France, and the Ph.D. degree in semiconductor electronics from the University of Essex, Colchester, U.K. He is currently holding a postdoctoral position in the Communications and Electronic Department, Telecom Paristech (former École Nationale Supérieure des Télécommunications) focused on the study of the dynamics of novel semiconductor laser sources



uniform circular array configurations to differentiate between interfering signals and a particular signal of interest. She joined the Ph.D. program at TELECOM Paris Tech in September 2015. Her thesis is focused on advanced laser diodes using new materials in particular those with III–V on silicon, nonlinear dynamics and optical chaos in semiconductor laser systems. She was with the US Army RDECOM Armament Research, Development, and Engineering Center where she served as a Project Officer in the Acoustic and Networked Sensor Division with specific program responsibility in the development of advanced acoustic sensors. She has a strong foundation in systems engineering and extensive experience in defense acquisition, program management, and life cycle support.

Sandra Gomez received the Bachelor's and Master's degrees in electrical engineering from Stevens Institute of Technology, Hoboken, NJ, USA, with a concentration in digital signal processing (DSP). She is currently the Technical Director of the International Technology Center, France, part of the US Army Research, Development, and Engineering Command (RDECOM) Forward Element Center Atlantic, Paris, France. She previously studied acoustic source localization and the tradeoffs of conventional and adaptive beamforming techniques using different

Antonin Gallet received the Master's degree of science from Ecole Normale supérieure de Cachan, Cachan, France, and the Master's degree of engineering from Institut d'optique, Palaiseau, France, in 2015. He started the Ph.D. research with III–V Lab, Palaiseau, France, and Télécom Paristech, Paris, France, in December 2015 to work on III–V/SOI lasers.

615
616
617
618
619
620
621
622
623
624
625
626
627
628
629
630
631
632
633
634



Guang-Hua Duan (S'88–M'90–SM'01) received the Doctorate degree in applied physics from the École Nationale Supérieure des Télécommunications (Telecom ParisTech), Paris, France, in 1991. He was habilitated to direct researches by Université de Paris-Sud in 1995. He is currently the Leader of the research team Silicon Photonics within III–V Lab, which is a joint laboratory of Nokia, Thales, and CEA Leti, and also the Head of the Research Department Heterogeneous integration of III–V on silicon within Nokia Bell Labs. He is also a Guest Professor in Ecole

Supérieure d'Électricité, and École Supérieure d'Optique, giving lectures in the fields of electromagnetism, optoelectronics, and laser physics. Previously, he was an Assistant, then an Associate Professor at Télécom-ParisTech from 1992 to 2000. He was with the University of Maryland as a Visiting Associate Professor from 1998 to 1999. He joined Opto+, Alcatel Research & Innovation Center in Marcoussis in October 2000. He is an author or coauthor of more than 100 journal papers, 250 conference papers, 30 patents, and a contributor to 4 book chapters.



Frédéric Grillot was born in Versailles, France, on August 22, 1974. He received the M.Sc. degree from the University of Dijon, Dijon, France, in 1999, and the Ph.D. degree from the University of Besançon, Besançon, France, in 2003. His doctoral research activities were conducted within the Optical Component Research Department, Alcatel-Lucent, working on the effects of the optical feedback in semiconductor lasers, and the impact this phenomenon has on optical communication systems. From 2003 to 2004, he was with the Institut d'Électronique Fondamentale

(University Paris-Sud) where he focused on integrated optics modeling and on Si-based passive devices for optical interconnects. From September 2004 to September 2012, he was with the Institut National des Sciences Appliquées as an Assistant Professor. From 2008 to 2009, he was also a Visiting Professor at the University of New-Mexico, Albuquerque, NM, USA, leading research in optoelectronics at the Center for High Technology Materials. Since October 2012, he has been working with Telecom Paristech (alias École Nationale Supérieure des Télécommunications), Paris, France, where he became an Associate Professor then a Full Professor in January 2017. Since August 2015, he has also been serving as a Research Professor at the University of New-Mexico. He is the author or coauthor of 77 journal papers, 1 book, 3 book chapters, and more than 170 contributions in international conferences and workshops. His current research interests include advanced quantum confined devices using new materials such as quantum dots and dashes, light emitters based on intersubband transitions, nonlinear dynamics and optical chaos in semiconductor lasers systems, as well as microwave and silicon photonics applications including photonic clocks and photonic analog-to-digital converters. He is an Associate Editor for *Optics Express*, a Senior Member of the SPIE and the IEEE Photonics Society, as well as a Member of the OSA.

635
636
637
638
639
640
641
642
643
644
645
646
647
648
649
650
651
652
653
654
655
656
657
658
659
660
661
662
663
664
665

IEEE PREPRINT

NOTICES

- 667 • Author: If you have not completed your electronic copyright form (ECF) and payment option please return to Scholar One
668 “Transfer Center.” In the Transfer Center you will click on “Manuscripts with Decisions” link. You will see your article details
669 and under the “Actions” column click “Transfer Copyright.” From the ECF it will direct you to the payment portal to select
670 your payment options and then return to ECF for copyright submission.
- 671 • Author: Please be aware that authors are required to pay overlength page charges \$220 per page if the paper is longer than 8
672 pages for Contributions and +12 pages for Invited Papers. If you cannot pay any or all of these charges please let us know.
- 673 • Author: This pdf contains 2 proofs. The first half is the version that will appear on Xplore. The second half is the version that
674 will appear in print. If you have any figures to print in color, they will be in color in both proofs.
- 675 • Author: The option to publish your paper as Open Access expires when the paper is fully published on Xplore. Only papers
676 published in “Early Access” may be changed to Open Access.

QUERIES

- 678 Q1. Author: If you have not completed your electronic copyright form (ECF) and payment option please return to Scholar One
679 “Transfer Center”. In the Transfer Center you will click on “Manuscripts with Decisions” link. You will see your article
680 details and under the “Actions” column click “Transfer Copyright”. From the ECF it will direct you to the payment portal to
681 select your payment options and then return to ECF for copyright submission.